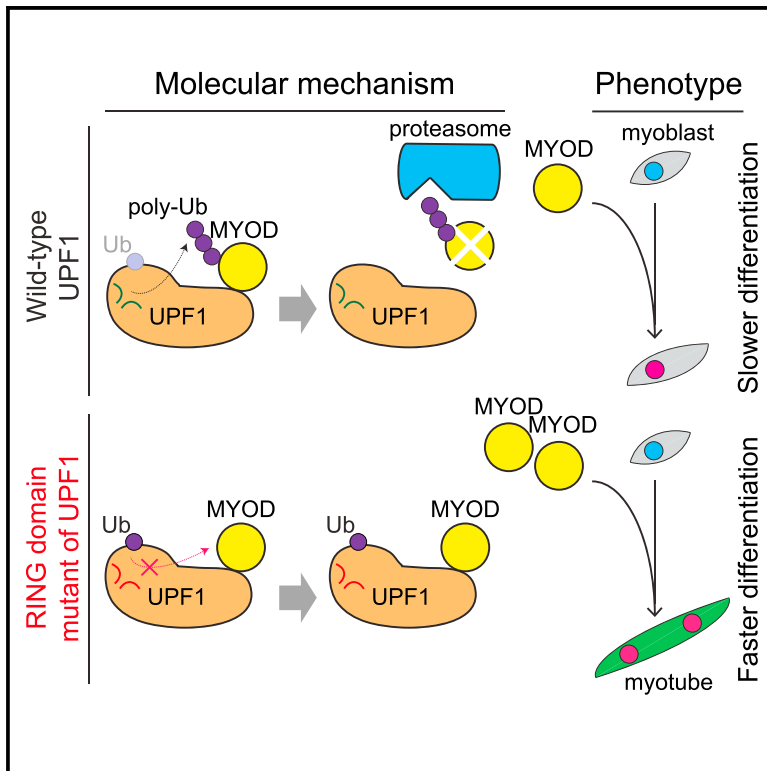


Molecular Cell

The RNA Surveillance Factor UPF1 Represses Myogenesis via Its E3 Ubiquitin Ligase Activity

Graphical Abstract



Authors

Qing Feng, Sujatha Jagannathan,
Robert K. Bradley

Correspondence

rbradley@fredhutch.org

In Brief

Feng et al. report that UPF1, a core RNA surveillance factor, represses human skeletal myogenesis. UPF1's repressive role in myogenesis is not explained by its well-studied RNA helicase activity. Instead, UPF1 has E3 ubiquitin ligase activity that targets MYOD protein, a master regulator of the myogenic process, for degradation.

Highlights

- *UPF1* knockdown accelerates myogenesis, while *UPF1* overexpression slows myogenesis
- UPF1 promotes MYOD protein decay, but it does not affect MYOD mRNA stability
- UPF1 has E3 ubiquitin ligase activity that targets MYOD protein for degradation
- Mutating UPF1's E3 ligase domain reverses UPF1's repressive role in myogenesis

The RNA Surveillance Factor UPF1 Represses Myogenesis via Its E3 Ubiquitin Ligase Activity

Qing Feng,^{1,2,3} Sujatha Jagannathan,^{1,2,4} and Robert K. Bradley^{1,2,5,*}

¹Computational Biology Program, Public Health Sciences Division, Fred Hutchinson Cancer Research Center, Seattle, WA 98109, USA

²Basic Sciences Division, Fred Hutchinson Cancer Research Center, Seattle, WA 98109, USA

³Molecular and Cellular Biology Graduate Program, University of Washington, Seattle, WA 98105, USA

⁴Human Biology Division, Fred Hutchinson Cancer Research Center, Seattle, WA 98109, USA

⁵Lead Contact

*Correspondence: rbradley@fredhutch.org

<http://dx.doi.org/10.1016/j.molcel.2017.05.034>

SUMMARY

UPF1 is an RNA helicase that orchestrates nonsense-mediated decay and other RNA surveillance pathways. While UPF1 is best known for its basal cytoprotective role in degrading aberrant RNAs, UPF1 also degrades specific, normally occurring mRNAs to regulate diverse cellular processes. Here we describe a role for UPF1 in regulated protein decay, wherein UPF1 acts as an E3 ubiquitin ligase to repress human skeletal muscle differentiation. Suppressing UPF1 accelerates myogenesis, while ectopically increasing UPF1 levels slows myogenesis. UPF1 promotes the decay of MYOD protein, a transcription factor that is a master regulator of myogenesis, while leaving MYOD mRNA stability unaffected. UPF1 acts as an E3 ligase via its RING domain to promote MYOD protein ubiquitination and degradation. Our data characterize a regulatory role for UPF1 in myogenesis, and they demonstrate that UPF1 provides a mechanistic link between the RNA and protein decay machineries in human cells.

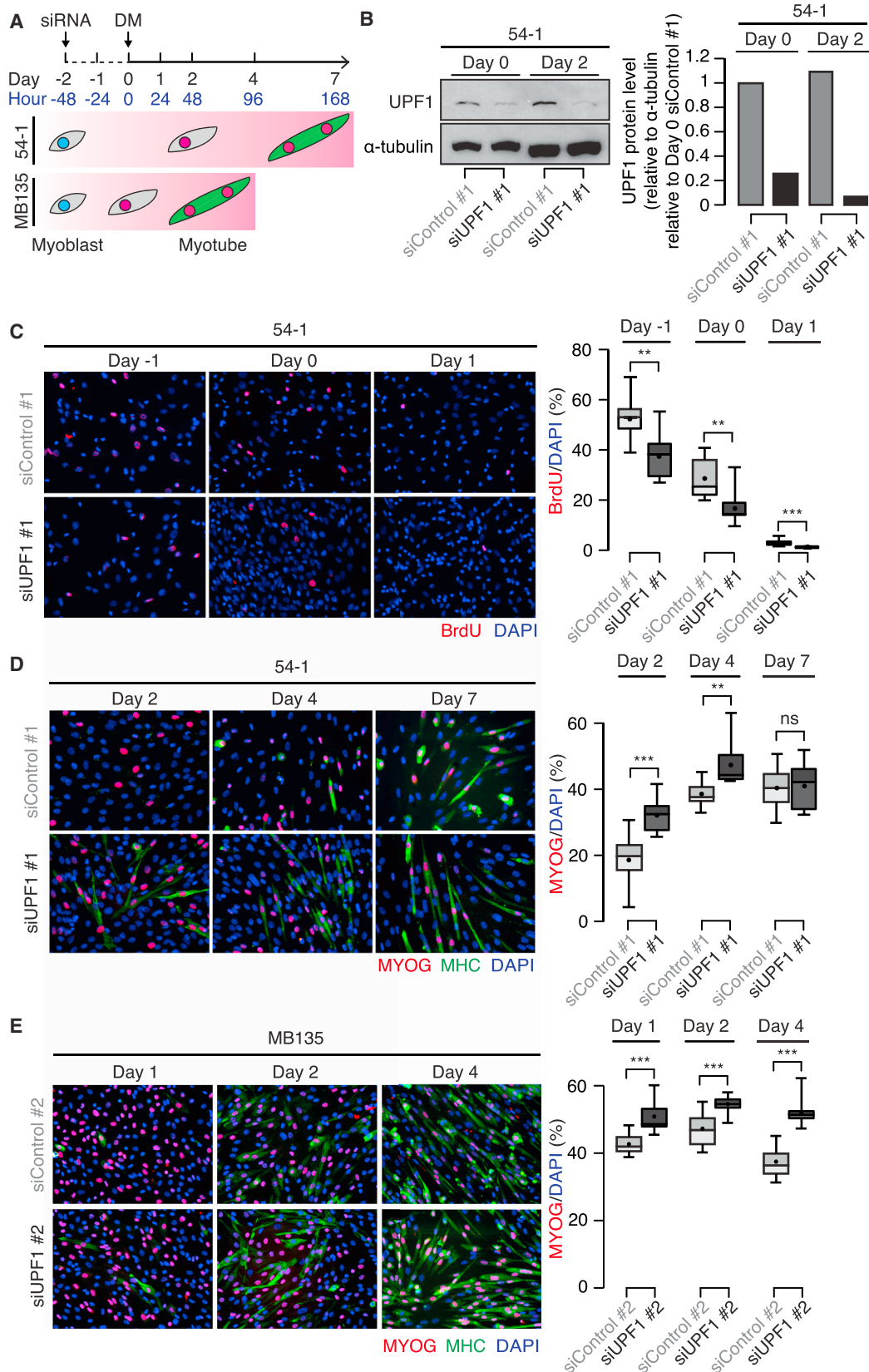
INTRODUCTION

Nonsense-mediated RNA decay (NMD) is a highly conserved post-transcriptional pathway that selectively degrades both abnormal and normally occurring RNA. NMD is best known for its role as an mRNA surveillance mechanism. In that capacity, NMD recognizes and degrades aberrant mRNAs containing premature termination codons that interrupt the normal reading frames of genes (Lykke-Andersen and Jensen, 2015; Popp and Maquat, 2013). Such aberrant mRNAs can arise from many sources, including genetic variation, somatic mutations, and errors introduced during RNA transcription or splicing. However, NMD is not just a cytoprotective pathway. In addition to suppressing aberrant RNAs, NMD also degrades many normally occurring mRNAs that contain sequence features that trigger NMD, including splice junctions downstream of stop codons, upstream open reading frames in the 5' UTR, or a long 3' UTR.

Approximately 10%–30% of normally occurring human mRNAs are predicted substrates for degradation by NMD (Hurt et al., 2013; Lewis et al., 2003; McIlwain et al., 2010).

By controlling the levels of many endogenous mRNAs, NMD can regulate diverse molecular processes in addition to functioning as a basal cytoprotective mechanism. For example, mRNAs encoding key effectors of the unfolded protein response are degraded by NMD (Karam et al., 2015), while endoplasmic reticulum stress in turn inhibits NMD (Wang et al., 2011). NMD also contributes to the regulation of the integrated stress response (Gardner, 2008; Martin and Gardner, 2015; Wang et al., 2011), apoptosis (Jia et al., 2015; Popp and Maquat, 2015), immune response (Gloggnitzer et al., 2014), response to viral infection (Balistreri et al., 2014; Ramage et al., 2015), and other core physiological processes. Ongoing attempts to identify endogenous NMD substrates will continue to reveal new regulatory roles for NMD.

The broad scope of NMD's regulatory role is exemplified by recent evidence that NMD factors regulate cell differentiation and cell fate. Many lines of evidence implicate NMD in differentiation. NMD efficiency, the fraction of an NMD substrate that is recognized and degraded instead of escaping degradation, varies during development and differentiation. NMD substrates are differentially recognized during *C. elegans* development, and NMD efficiency decreases during mammalian myogenesis and neurogenesis (Barberan-Soler et al., 2009; Bruno et al., 2011; Gong et al., 2009). Cellular requirements for NMD also vary during differentiation. Hematopoietic deletion of *Upf2*, encoding a core component of the NMD machinery, ablated hematopoietic stem and progenitor cells, but not more differentiated blood cells (Weischenfeldt et al., 2008). NMD is also required for licensing some cell types for differentiation. Deletion of *Smg6*, encoding an NMD factor with endonucleolytic activity, blocked the differentiation of mouse embryonic stem cells without impairing their proliferation (Li et al., 2015). Similarly, conditional deletion of *Upf2* prevented fetal liver cells from undergoing terminal differentiation (Thoren et al., 2010). Finally, NMD has been directly implicated in repressing neural differentiation. Overexpression or knockdown of *Upf1*, encoding an RNA helicase that is required for NMD, respectively inhibited or promoted murine neurogenesis. NMD influences neurogenesis in part by degrading the mRNA encoding SMAD7, which regulates neurogenesis via TGF- β signaling (Lou et al., 2014).



(legend on next page)

Muscle differentiation may represent a tractable and biomedically relevant system to study the role of NMD in cell differentiation for several reasons. First, a previous study reported that UPF1 levels and NMD efficiency decreased during skeletal myogenesis and that the mRNA encoding the myogenic marker Myogenin (MYOG) was degraded by NMD (Gong et al., 2009). These data suggest that NMD factors might repress myogenesis, although that hypothesis has not been tested. Second, the regulatory factors controlling muscle differentiation are well characterized, which may facilitate identifying direct mechanistic ties between NMD and master regulators of myogenesis. Third, we recently found that expression of the disease gene *DUX4* in skeletal muscle, which causes facioscapulohumeral muscular dystrophy, results in UPF1 protein degradation and severe inhibition of NMD (Feng et al., 2015). Determining the normal role of NMD during myogenesis is, therefore, of direct biomedical relevance.

In this study, we describe a direct and mechanistic role for the central NMD factor UPF1 in repressing human muscle differentiation. UPF1 promotes proteasome-mediated degradation of MYOD protein, a master regulator of the myogenic process. UPF1 promotes MYOD proteolysis by acting as an E3 ubiquitin ligase via its RING domain while leaving MYOD mRNA stability unaffected. Mutating UPF1's RING domain alleviates UPF1-dependent MYOD proteolysis and reverses UPF1's repressive role in myogenesis.

RESULTS

UPF1 Knockdown Accelerates Human Myogenesis

To determine whether the reported decrease in UPF1 levels and NMD efficiency that occurs during myogenesis (Gong et al., 2009) plays a regulatory and causative role, rather than being a by-product of the myogenic process, we tested whether forced reductions in UPF1 levels altered the efficiency of myoblast differentiation. We transfected two genetically distinct myoblast cell lines generated from healthy human muscle (54-1 and MB135 cells) with two different small interfering RNAs (siRNAs) against UPF1, reducing UPF1 protein to 24.7% and 63.0% of levels in cells transfected with two different non-targeting siRNAs (Figures 1A, 1B, and S1A–S1C). We induced differentiation 2 days post-transfection (day 0) by switching the confluent myoblasts from high-serum growth media to low-serum differen-

tiation media, which promotes cell cycle stalling and the expression of myogenic markers.

UPF1 knockdown (KD) resulted in accelerated differentiation throughout the myogenic process in both 54-1 and MB135 myoblasts. We first analyzed cells from the 54-1 genetic background, finding that UPF1 KD promoted cell cycle exit even prior to the initiation of differentiation. One day after transfection with control versus UPF1-targeting siRNAs (day –1), 52.2% versus 37.8% of nuclei were bromodeoxyuridine (BrdU)+ (Figure 1C). We then quantified muscle differentiation by counting the fraction of nuclei expressing MYOG, a marker of myogenic commitment. At 2 days post-induction of differentiation (day 2), we observed 68.7% more MYOG+ nuclei in UPF1-KD cells compared to control cells, coincident with a 3.5-fold increase in MYOG mRNA (Figures 1D and S1D). This increase in MYOG occurred only after the induction of differentiation. UPF1-KD cells matured faster into myotubes marked by myosin heavy chain (MHC) expression, with MHC staining readily visible at day 2 when essentially none was evident in control cells. The same phenotype of accelerated myogenesis occurred in MB135 myoblasts, which differentiate more rapidly than do the genetically distinct 54-1 myoblasts, following transfection with a distinct siRNA against UPF1 (Figures 1E and S1E).

We next confirmed that UPF1 KD drives accelerated myogenesis in the physiological setting of primary, rather than immortalized, cell differentiation. We repeated the above differentiation experiments with two genetically distinct cultures of primary human skeletal muscle cells. These primary MB135 and MB2401 myoblasts were obtained from muscle biopsies of two healthy individuals. (A different culture of primary MB135 cells was previously immortalized to generate the immortalized MB135 cell line used in this study.) Transduction with UPF1-targeting small hairpin RNAs (shRNAs) resulted in efficient UPF1 KD and accelerated myogenesis (Figures S1F–S1H). We concluded that ectopic suppression of UPF1 levels promotes differentiation of both immortalized and primary human myoblasts.

UPF1 Overexpression Slows Myogenesis

As UPF1 KD accelerated myogenesis, we hypothesized that UPF1 overexpression might conversely slow myogenesis. To test this hypothesis, we generated a clonal myoblast cell line in the MB135 genetic background that expressed doxycycline (Dox)-inducible FLAG-tagged UPF1 (Figure 2A). We induced

Figure 1. UPF1 KD Accelerates Myoblast Differentiation

(A) Schematic of a time course of human myoblast differentiation following UPF1 knockdown (KD). Two genetically distinct human myoblast cell lines (54-1 and MB135 cells) were transfected with two different siRNAs against UPF1, as well as two different non-targeting siRNAs as controls (day –2). When the transfected cells reached full confluency (day 0), differentiation was induced by switching from high-serum growth media to low-serum differentiation media (DM). 54-1 and MB135 cells respectively differentiate less and more rapidly, and so were differentiated for 7 and 4 days, respectively.

(B) Immunoblot for UPF1 protein from 54-1 cells following control or UPF1 KD immediately prior to (day 0) or 2 days after (day 2) induction of differentiation. Equal amounts of protein were loaded based on the bicinchoninic acid (BCA) assay. α -tubulin, loading control; bar plot, quantification of UPF1 protein levels relative to the loading control.

(C) Immunofluorescence labeling of 54-1 cells with an antibody against BrdU (red) at the indicated time points, prior to significant cell fusion. At each time point, cells were fixed after 1 hr of BrdU labeling. Boxplot, percentage of BrdU+ nuclei measured over ten fields; whiskers, maximum and minimum over the fields. * $p < 0.05$, ** $p < 0.01$, *** $p < 0.001$.

(D and E) Immunofluorescence labeling of 54-1 or MB135 cells with antibodies against Myogenin (MYOG, red) and myosin heavy chain (MHC, green) at the indicated time points. MB135 cells differentiate more rapidly than 54-1 cells do and so a shorter time course was used. Boxplot, percentage of MYOG+ nuclei measured over ten fields; whiskers, maximum and minimum over the fields. * $p < 0.05$, ** $p < 0.01$, *** $p < 0.001$.

See also Figure S1.

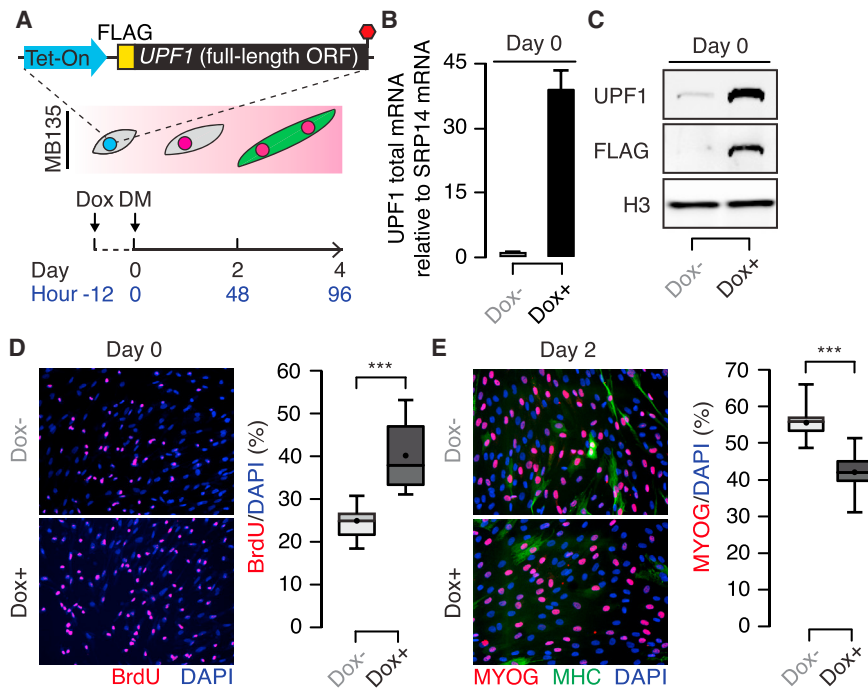


Figure 2. UPF1 Overexpression Slows Myoblast Differentiation

(A) Schematic illustrating a time course of human myoblast differentiation following the induction of *UPF1* overexpression in MB135 myoblasts. Transgenic *UPF1* was induced or not induced 12 hr prior to the induction of differentiation.

(B) Levels of *UPF1* mRNA at day 0, 12 hr after the addition of Dox to induce *UPF1* expression. Error bars, SD.

(C) Immunoblot for total and transgenic *UPF1* protein at the same time point as in (B), measured using antibodies against *UPF1* and FLAG. H3, loading control histone H3.

(D) Immunofluorescence labeling with an antibody against BrdU (red) at day 0. Cells were fixed and labeled after incubation with BrdU-containing media for 1 hr. Boxplot, percentage of BrdU+ nuclei measured over eight fields; whiskers, maximum and minimum over the fields. * $p < 0.05$, ** $p < 0.01$, *** $p < 0.001$.

(E) Immunofluorescence labeling with antibodies against MYOG (red) and MHC (green) at day 2. Boxplot, percentage of MYOG+ nuclei measured over ten fields; whiskers, maximum and minimum over the fields. * $p < 0.05$, ** $p < 0.01$, *** $p < 0.001$.

UPF1 overexpression by adding Dox to the media 12 hr prior to the induction of differentiation, resulting in robust 46- and 16-fold increases in *UPF1* mRNA and protein levels (Figures 2B and 2C). Consistent with our hypothesis, *UPF1* overexpression reversed both the cell cycle and myogenic phenotypes observed following *UPF1* KD. *UPF1*-overexpressing cells contained 40.3% BrdU+ nuclei versus 24.7% for control (uninduced) cells at day 0, immediately prior to the induction of differentiation (Figure 2D). *UPF1*-overexpressing versus control cells similarly exhibited 41.6% versus 55.3% MYOG+ nuclei at day 2, 2 days post-differentiation (Figure 2E). Taken together, our *UPF1* KD and overexpression experiments indicate that *UPF1* represses myogenesis through an unknown mechanism.

UPF1 KD Induces the MYOD Transcriptional Program

We next sought to determine the molecular mechanism by which *UPF1* represses myogenesis. NMD represses diverse targets, including the gene encoding the marker of myogenic commitment, MYOG (Gong et al., 2009). MYOG exhibits higher mRNA and protein levels 2 days after the induction of differentiation, but not before (Figures 1D, 1E, S1D, and S1E). We therefore hypothesized that *UPF1* might repress myogenesis by targeting the mRNA of a key earlier myogenic factor for degradation.

To identify myogenic regulatory factors that might connect *UPF1* levels to the myogenic process, we characterized the transcriptomes of cells following *UPF1* or control KD with RNA sequencing (RNA-seq) 2 days post-differentiation. Coding genes that were upregulated by ≥ 1.5 -fold (365 genes) following *UPF1* versus control KD were strongly enriched for myogenic processes in a gene ontology analysis, consistent with the cellular myogenic phenotype induced by *UPF1* KD (Figures 3A and

3B). Subsequent analysis revealed that 6.6% of these upregulated genes were known direct targets of the transcription factor MYOD, a master myogenic factor that is one of the earliest factors that initiates myogenesis and whose expression is sufficient to transdifferentiate fibroblasts into myoblasts (Tapscott et al., 1988). Furthermore, 13 of the upregulated genes were MYOD-specific targets that are not promoted by other early myogenic transcription factors (Figure 3C). Global gene expression patterns following *UPF1* KD therefore indicate that *UPF1* KD activates the MYOD transcriptional cascade. Consistent with MYOD playing a central role in driving accelerated myogenesis following *UPF1* KD, we observed a 2.7-fold increase in MYOD protein 24 hr after *UPF1* KD, prior to the induction of differentiation (Figure 3D).

UPF1 KD Induces MYOD Protein, yet Does Not Stabilize MYOD mRNA

Given *UPF1*'s central role in RNA surveillance, we hypothesized that *UPF1* KD alleviated NMD-dependent degradation of the MYOD mRNA to promote increased MYOD protein levels. Two predictions follow from this hypothesis. First, MYOD mRNA levels should increase before or at the same time as MYOD protein levels do following *UPF1* KD. Second, MYOD mRNA should be stabilized by *UPF1* KD. To our surprise, neither prediction was correct. First, a time course revealed that MYOD protein upregulation (which occurs between -30 and -27 hr) occurred 15–18 hr prior to MYOD mRNA upregulation (which occurs between -24 and -12 hr) following *UPF1* KD (red arrow, Figures 4A–4C). Second, measurement of the MYOD mRNA half-life revealed that MYOD mRNA was not stabilized by *UPF1* KD at day 0 despite clearly evident mRNA upregulation (Figure 4D). We observed the same pattern, wherein MYOD protein upregulation occurred

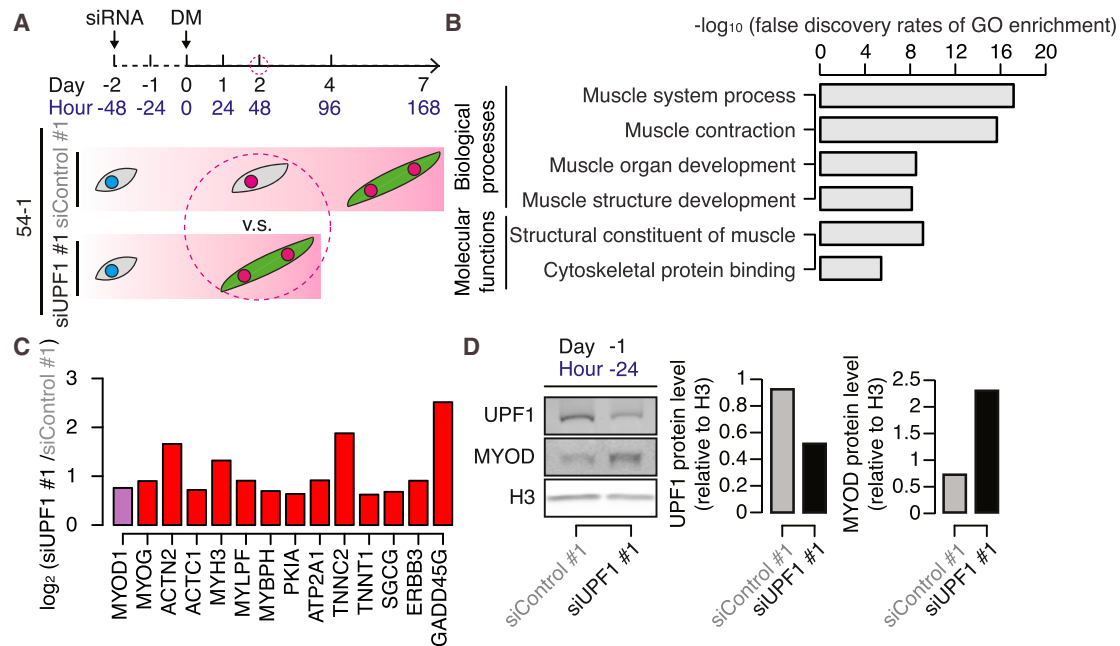


Figure 3. *UPF1* KD Promotes a Myogenic Gene Expression Program, Including MYOD-Specific Targets

(A) Schematic illustrating when RNA was collected for RNA-seq (day 2) during differentiation of 54-1 myoblasts following control or *UPF1* KD. (B) Gene ontology (GO) enrichment analysis of genes that were upregulated by ≥ 1.5 -fold following *UPF1* versus control KD at day 2. (C) Relative mRNA levels of genes that are specifically activated by MYOD and not other myogenic factors (red) (Conerly et al., 2016; Ishibashi et al., 2005), as well as MYOD mRNA itself (purple), following *UPF1* versus control KD at day 2. The illustrated genes exhibited increases in expression of ≥ 1.5 -fold. (D) Immunoblots for UPF1 and MYOD proteins 1 day following transfection with a control or *UPF1*-targeting siRNA (day -1, or equivalently hr -24), 1 day prior to the induction of differentiation. H3, loading control histone H3; bar plots, quantification of UPF1 and MYOD relative to the loading control.

10–18 hr prior to MYOD mRNA upregulation, following *UPF1* KD in MB135 cells (Figure S2).

Increased levels of MYOD mRNA following *UPF1* KD are likely due to MYOD transcriptional upregulation rather than alleviation of post-transcriptional repression. We observed similar increases in pre-mRNA and mature mRNA transcribed from *MYOD* following control versus *UPF1* KD, consistent with MYOD transcriptional upregulation (Figure 4E). Our data therefore indicate that *UPF1* KD activates the MYOD transcriptional cascade, but they do not support our original hypothesis that *UPF1* represses myogenesis by regulating MYOD mRNA levels. In contrast, *UPF1* KD induces MYOD protein while leaving its mRNA unaffected.

UPF1 Regulates MYOD Protein via the Proteasome

We next sought to determine the molecular mechanism by which *UPF1* KD resulted in upregulation of MYOD protein. As we observed increased MYOD protein prior to the upregulation of MYOD mRNA following *UPF1* KD, we hypothesized that *UPF1* might repress MYOD protein by mediating MYOD proteolytic decay. To test this hypothesis, we returned to the inducible *UPF1* overexpression system. Just as *UPF1* KD induced MYOD protein, so did *UPF1* overexpression result in decreased MYOD protein. MYOD protein levels decreased to 25.7% of their original levels within 12 hr of the addition of Dox to induce *UPF1* overexpression (Figures 5A and 5B). *UPF1*-dependent suppression of MYOD protein was prevented when we treated cells with

the proteasome inhibitor MG132 (Figure 5C). We concluded that *UPF1* represses MYOD protein in a proteasome-dependent manner.

UPF1 Represses MYOD Protein via Its E3 Ubiquitin Ligase Activity

How does *UPF1* repress MYOD protein? As *UPF1*-mediated repression of MYOD protein is proteasome dependent (Figure 5C), we hypothesized that *UPF1* promoted MYOD protein decay via an unknown mechanism. Although this mechanism could conceivably be indirect—for example, mediated by *UPF1*-dependent degradation of an mRNA encoding an E3 ubiquitin ligase that targets MYOD protein—three pieces of evidence led us to hypothesize a direct role for *UPF1* in directing MYOD proteolysis. First, MYOD protein levels decreased concordantly with increased *UPF1* expression, without the temporal lag expected of an indirect mechanism dependent upon mRNA stabilization of a tertiary factor (Figure 5B). Second, in addition to its RNA helicase domain, *UPF1* possesses an N-terminal cysteine- and histidine-rich domain that is structurally similar to the RING domains frequently found in E3 ubiquitin ligases (Kadlec et al., 2006). Yeast *Upf1* can self-ubiquitinate in vitro, suggesting that its RING-like domain functions as an E3 ligase, although it is unknown whether this E3 activity occurs in vivo or in human cells (Takahashi et al., 2008). Third, previous proteomic studies of the *UPF1* interactome recovered components of the ubiquitin-proteasome system (Brannan et al., 2016; Flury et al., 2014).

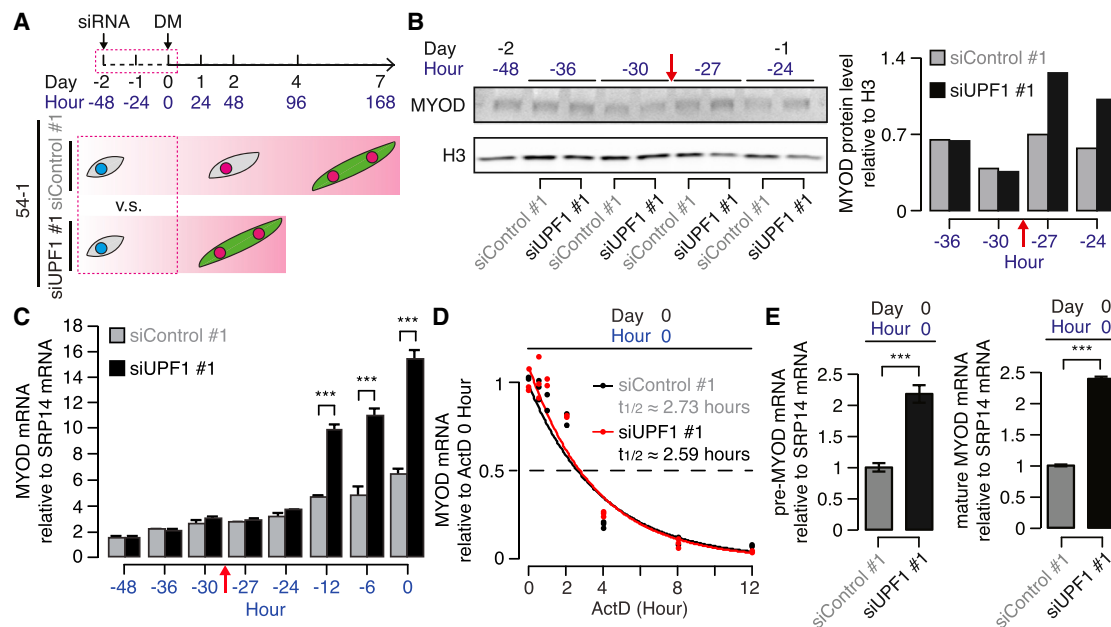


Figure 4. UPF1 KD Induces MYOD Protein in the Absence of MYOD mRNA Upregulation

(A) Schematic illustrating time points for sample collection following *UPF1* KD (day -2 to 0 , or equivalently hr -48 to 0) in 54-1 myoblasts. (B) Immunoblot for MYOD protein in the 24 hr immediately following transfection with a control or *UPF1*-targeting siRNA (day -2 to day -1 , or equivalently hr -48 to -24). Red arrow indicates when MYOD protein levels detectably increased (between hr -30 and -27). H3, loading control histone H3; bar plot, quantification of MYOD protein relative to the loading control. (C) Relative levels of MYOD mRNA in the 48 hr immediately following transfection with a control or *UPF1*-targeting siRNA (day -2 to day 0 , or equivalently hr -48 to 0). Red arrow indicates when MYOD protein levels detectably increased (see B). * $p < 0.05$, ** $p < 0.01$, *** $p < 0.001$. (D) Estimates of MYOD mRNA half-lives at day 0 (hr 0) in control or *UPF1*-KD cells. MYOD mRNA levels were measured 0, 0.5, 1, 2, 4, 8, and 12 hr after the addition of actinomycin D (ActD, 2.5 $\mu\text{g}/\text{mL}$) to inhibit transcription. (E) Relative levels of MYOD pre-mRNA (left) and mature mRNA (right) at day 0 (hr 0) in control or *UPF1*-KD cells, normalized to MYOD pre-mRNA or mature mRNA levels in control KD samples. Error bars, error propagation computed with the balanced repeated replication (BRR) method. * $p < 0.05$, ** $p < 0.01$, *** $p < 0.001$. See also Figure S2.

We therefore sought to test the hypothesis that human UPF1's RING-like domain is responsible for repressing MYOD protein.

We first confirmed that the structure of human UPF1's RING domain is consistent with the E3 ubiquitin ligase activity reported for yeast Upf1. UPF1's RING domain resides near UPF1's N terminus and consists of two zinc fingers that were previously reported to provide a peripheral surface for UPF2 binding (Kadlec et al., 2006). We took advantage of a crystal structure of full-length UPF1 in complex with a C-terminal portion of UPF2 (Clerici et al., 2009), and we compared the 2D and 3D structures of UPF1's RING domain to the structures of known RING E3 ubiquitin ligases. This comparison revealed that the two zinc fingers that comprise UPF1's RING domain are consistent with the canonical binding pocket formed by loops one and two of functional RING domains. This binding pocket of functional RING domains mediates interactions with E2 ubiquitin-conjugating proteins (Berndsen and Wolberger, 2014; Lorick et al., 1999; Metzger et al., 2014) (Figures 6A–6C). We concluded that UPF1's structure likely contains the E2-E3 binding pocket expected of a functional E3 ligase.

We sought to mutate UPF1's RING domain in order to reduce its putative E3 activity while leaving its NMD activity intact. We constructed the mutant UPF1^{S124A/N138A/T139A} by mutating three

residues within loops one and two into alanine, with the goal of disrupting UPF1's putative E2-binding pocket. These residues (S124/N138/T139) are proximal, but not identical, to the highly conserved cysteines and serine that are responsible for zinc ion coordination (C123 and C126 within loop one and C137 and S140 within loop two). We did not mutate Y125 because it is responsible for holding the two α helices on the RING domain periphery. We generated clonal MB135 myoblasts that inducibly expressed UPF1^{S124A/N138A/T139A}, and we compared these cells to our previously generated cells that inducibly expressed wild-type UPF1 (UPF1^{WT}). The UPF1^{WT} and UPF1^{S124A/N138A/T139A} transgenes exhibited comparable UPF1 mRNA induction upon Dox treatment, and they produced similar levels of FLAG-tagged UPF1 protein (Figure 6D).

We first confirmed that mutating UPF1's RING domain did not compromise its NMD activity. We measured levels of three endogenous NMD substrates in myoblasts overexpressing either wild-type or mutant UPF1. Overexpression of UPF1^{S124A/N138A/T139A} did not substantially alter levels of these endogenous NMD substrates relative to overexpression of UPF1^{WT} (Figure S3A). As we overexpressed mutant UPF1 in the context of endogenous (wild-type) UPF1 expression, these data demonstrate that UPF1^{S124A/N138A/T139A} is not a dominant

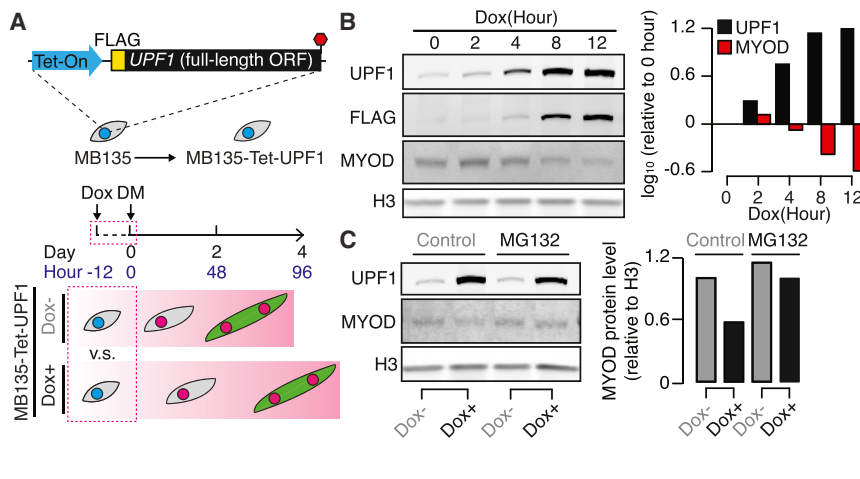


Figure 5. UPF1 Promotes Proteasome-Dependent Degradation of MYOD Protein

(A) Schematic illustrating a time course of differentiation following the induction of *UPF1* overexpression in MB135 myoblasts. Samples were collected during the 12 hr immediately following Dox treatment (hr -12 to 0).

(B) Immunoblot for total *UPF1*, FLAG-tagged transgenic *UPF1*, and *MYOD* proteins, measured during the 12 hr following Dox treatment. H3, loading control histone H3; bar plot, quantification of total *UPF1* and *MYOD* proteins relative to the loading control.

(C) Immunoblot for total *UPF1* and *MYOD* proteins, measured 12 hr after Dox treatment, in cells treated with the proteasome inhibitor MG132 (10 μ M, 8-hr treatment). H3, loading control histone H3; bar plot, quantification of *MYOD* protein relative to the loading control.

negative for NMD activity, but they do not test whether *UPF1*^{S124A/N138A/T139A} itself can function in NMD. We therefore specifically knocked down endogenous *UPF1* with an shRNA targeting the 3' UTR of *UPF1* (which was not present in our transgenes), induced expression of *UPF1*^{WT} or *UPF1*^{S124A/N138A/T139A}, and measured levels of endogenous NMD substrates (Figures S3B and S4). NMD substrate levels were not significantly higher in *UPF1*^{S124A/N138A/T139A}-expressing versus *UPF1*^{WT}-expressing cells following endogenous *UPF1* KD. These data suggest that *UPF1*^{S124A/N138A/T139A} is competent for NMD and, therefore, is useful for our goal of deconvolving *UPF1*'s NMD and putative E3 ligase activities.

We next tested whether the S124A/N138A/T139A mutation had the intended effect of disrupting *UPF1*'s putative E2 ubiquitin conjugase-binding pocket. The yeast E2 conjugase Ubc3 was previously reported to be a binding/activation partner for yeast Upf1's E3 ligase activity (Takahashi et al., 2008). We therefore tested whether our RING domain mutation affected possible interactions between *UPF1* and the E2 conjugase CDC34, the human ortholog of yeast Ubc3. Immunoprecipitation of FLAG-tagged *UPF1* followed by immunoblotting against HA-tagged CDC34 revealed that *UPF1* interacts with CDC34. The S124A/N138A/T139A mutation attenuated, but did not abolish, this interaction (Figure S3C). Suggestively, the E2 ubiquitin conjugase activity of CDC34 has been previously implicated in *MYOD* protein turnover (Song et al., 1998).

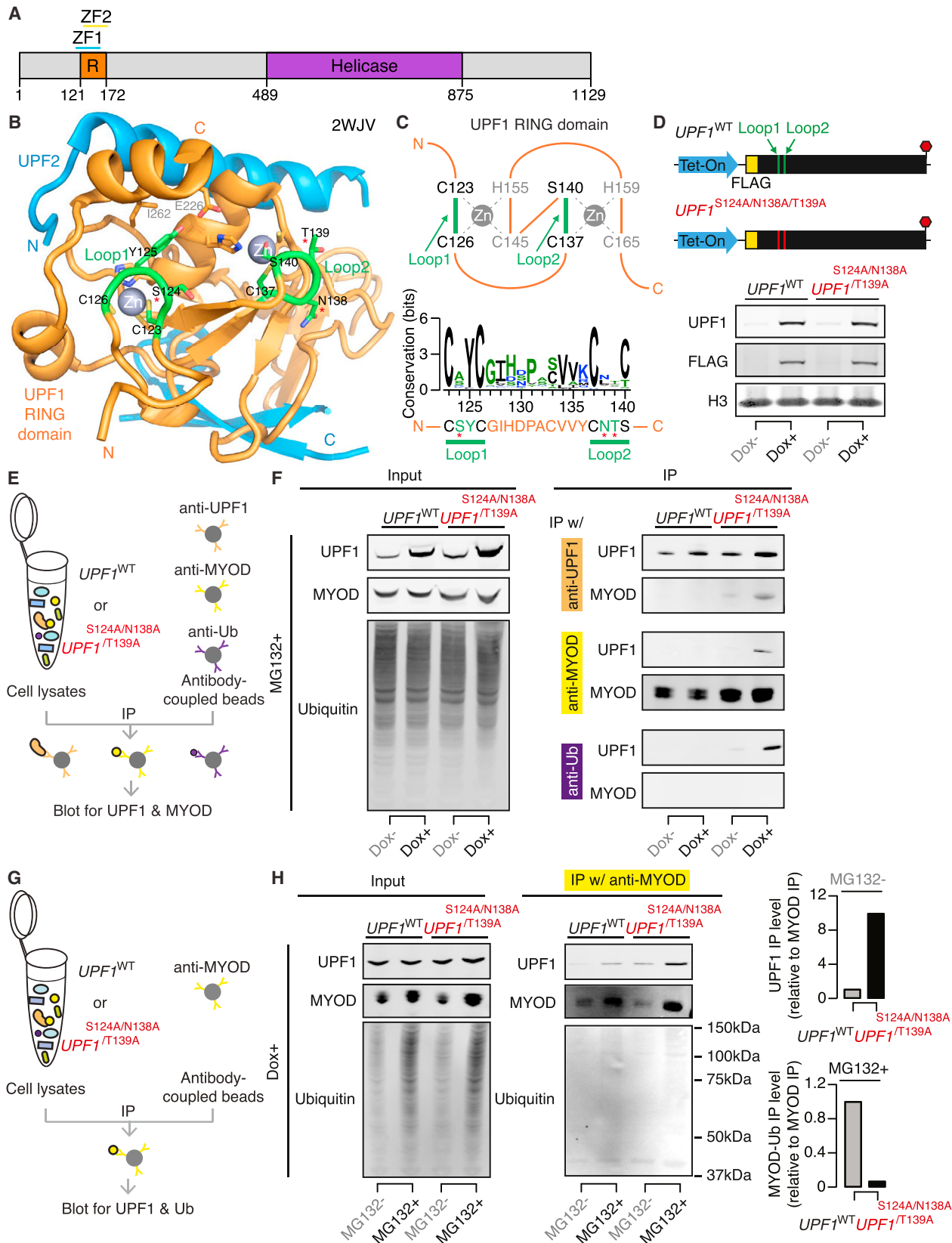
We sought to determine the specific mechanistic consequence of the S124A/N138A/T139A mutation for *UPF1*'s putative E3 ligase activity. The RING domains of many well-characterized E3 ligases are commonly involved in recruiting an E2 conjugase as well as transferring ubiquitin to the substrate, whereas other domains of the E3 ligases or co-factors govern substrate specificity (Berndsen and Wolberger, 2014; Deshaies and Joazeiro, 2009; Lorick et al., 1999; Lydeard et al., 2013; Skaar et al., 2013). As *UPF1*^{S124A/N138A/T139A} exhibited reduced binding to the E2 conjugase CDC34 that was previously implicated in *MYOD* ubiquitination, we hypothesized that *UPF1*^{S124A/N138A/T139A} would also exhibit reduced activity for ubiquitin transfer to the candidate substrate *MYOD*. This hypothesis generated several testable predictions. First, we expected

UPF1 and *MYOD* to interact physically. Second, we expected *UPF1*^{S124A/N138A/T139A}, but not *UPF1*^{WT}, to remain charged with mono-ubiquitin upon proteasome inhibition. Third, we expected *MYOD* ubiquitination to decrease in *UPF1*^{S124A/N138A/T139A}-expressing cells relative to *UPF1*^{WT}-expressing cells. We systematically tested these hypotheses.

We collected cell lysates from *UPF1*^{WT}- or *UPF1*^{S124A/N138A/T139A}-expressing cells following proteasome inhibition; immunoprecipitated *UPF1*, *MYOD*, or ubiquitin; and probed for *UPF1* and *MYOD*. *UPF1*^{S124A/N138A/T139A} and *MYOD* robustly co-immunoprecipitated while *UPF1*^{WT} and *MYOD* interacted weakly. Immunoprecipitating ubiquitin revealed mono-ubiquitin associated with *UPF1*^{S124A/N138A/T139A}, but not *UPF1*^{WT} (Figures 6E and 6F). We next compared *MYOD* ubiquitination in *UPF1*^{WT}- and *UPF1*^{S124A/N138A/T139A}-expressing cells. *MYOD* poly-ubiquitination was readily visible upon proteasome inhibition in *UPF1*^{WT}-expressing cells, but not in *UPF1*^{S124A/N138A/T139A}-expressing cells (Figures 6G and 6H). These data suggest that the RING domain mutation S124A/N138A/T139A reduces *UPF1*'s E3 activity by compromising the transfer of ubiquitin to substrates. The increased physical interaction between *MYOD* and *UPF1*^{S124A/N138A/T139A} versus *UPF1*^{WT} suggests, although does not prove, that release of *MYOD* from its association with *UPF1* may be coupled to ubiquitin transfer. We concluded that *UPF1* ubiquitinates *MYOD* in vivo.

UPF1 Represses Myogenesis via Its RING Domain

We next tested whether mutating *UPF1*'s RING domain reduced *UPF1*-mediated *MYOD* protein degradation and accompanying repression of myogenesis. We treated *UPF1*^{WT} and *UPF1*^{S124A/N138A/T139A} cells with Dox to induce transgenic *UPF1* expression, and we measured *MYOD* protein stability following treatment with the translation inhibitor cycloheximide. Induction of *UPF1*^{WT} resulted in the rapid degradation of *MYOD* relative to uninduced cells while induction of *UPF1*^{S124A/N138A/T139A} did not. *MYOD* protein levels were reduced 6.5-fold in Dox-induced *UPF1*^{WT} cells relative to uninduced *UPF1*^{WT} cells 6 hr after cycloheximide treatment, but they were only reduced by 1.5-fold in induced relative to uninduced *UPF1*^{S124A/N138A/T139A} cells (Figure 7A).



(legend on next page)

Consistent with UPF1^{S124A/N138A/T139A}'s impaired ability to ubiquitinate MYOD, expression of UPF1^{S124A/N138A/T139A} reversed the anti-myogenic phenotype associated with UPF1^{WT} expression. Induction of UPF1^{WT} slowed myogenesis, while induction of UPF1^{S124A/N138A/T139A} caused a modest but statistically significant increase in myogenesis. Cells expressing UPF1^{S124A/N138A/T139A} versus UPF1^{WT} exhibited a higher fraction of MYOG+ nuclei and a 2.5-fold increase in MYOG mRNA levels (Figures 7B and S4).

As the above experiments were conducted in the presence of endogenous (wild-type) *UPF1*, we speculated that the phenotypic consequences of UPF1^{S124A/N138A/T139A} expression might be augmented when endogenous *UPF1* was suppressed. We therefore measured the kinetics of differentiation of UPF1^{S124A/N138A/T139A} versus UPF1^{WT}-expressing myoblasts in the context of endogenous *UPF1* KD. At 2 days after the induction of differentiation, we observed a 10.4-fold increase in MYOG levels in cells expressing UPF1^{S124A/N138A/T139A} versus UPF1^{WT} in the context of endogenous *UPF1* KD. In contrast, we observed a 2.5-fold increase in the context of unperturbed endogenous *UPF1* expression (Figure S4). We concluded that UPF1's RING domain is responsible for UPF1-mediated proteolysis of MYOD as well as UPF1's repressive role in myogenesis (Figure 7C).

DISCUSSION

Recent studies provided clear evidence that UPF1 contributes to the regulation of cell differentiation and fate choice by selectively degrading mRNAs encoding key differentiation factors. Our data complement these previous reports by implicating UPF1 in regulating the kinetics of myogenesis. Surprisingly, however, UPF1 influences myogenesis by promoting protein, rather than mRNA, degradation. Given UPF1's central role in nonsense-mediated decay and other RNA surveillance pathways, our findings therefore imply that UPF1 directly connects the RNA and protein decay machineries.

Given MYOD's role as initiator of the myogenic cascade (Tapscott et al., 1988), our data strongly suggest that UPF1-dependent ubiquitination of MYOD explains how UPF1 represses myogenesis. Consistent with this hypothesis, mutations in UPF1's RING domain that prevented UPF1-mediated MYOD ubiquitination also alleviated UPF1's repressive role in myogenesis (Figure 7). However, we cannot rule out the possibility that UPF1 ubiquitinates factors in addition to MYOD, which may contribute to UPF1's repressive role in myogenesis.

Similarly, it is possible that UPF1 influences MYOD protein levels via mechanisms in addition to the ubiquitination characterized here. For example, UPF1 could potentially repress MYOD mRNA translation through an unknown mechanism. However, our data indicate that UPF1 primarily represses MYOD at the level of protein turnover rather than translation for two reasons. First, UPF1-dependent suppression of MYOD protein is proteasome dependent (Figure 5C). Second, the 3-fold increase in MYOD protein that occurs upon *UPF1* KD (Figure 3D) is mimicked by the expression of our UPF1^{S124A/N138A/T139A} E3 ligase mutant, which results in an increase in MYOD protein stability of a similar magnitude (Figure 7A).

In many contexts, UPF1's capacities to promote RNA as well as protein degradation may be closely linked rather than disjoint biochemical activities. For example, UPF1's E3 activity may contribute to the degradation of abnormal and potentially deleterious peptides encoded by NMD substrates. Previous studies in yeast found that peptides encoded by reporter NMD substrates were degraded by the proteasome and that Upf1 was important for this process (Kuroha et al., 2009, 2013; Verma et al., 2013). However, the method by which Upf1 promoted selective degradation of such peptides was not identified. We hypothesize that UPF1's combined RNA helicase and E3 ligase activities might be directly responsible for recognizing NMD substrates as well as catalyzing the ubiquitination and degradation of the encoded peptides or proteins. However, further work is required to identify the spectrum of peptide products encoded by NMD substrates

Figure 6. UPF1's RING Domain Has E3 Ubiquitin Ligase Activity

- (A) Schematic of UPF1's protein domain structure (Kadlec et al., 2006; UniProt Consortium, 2012). Orange, RING-like domain; purple, RNA helicase domain.
- (B) Protein structure of UPF1's RING domain 1 (orange, residues 121–172 from PDB: 2WJV; Clerici et al., 2009), illustrating two zinc fingers coordinating zinc ions (gray spheres), the canonical E2-RING E3 interaction pocket formed by Loop1 and Loop2 (green) that faces inside, and the UPF2- (cyan) binding surface on the periphery. Structure was visualized with PyMOL (PyMOL Molecular Graphics System, Schrödinger).
- (C) Top: schematic diagram of UPF1's RING domain 1 (orange, residues 121–172 from PDB: 2WJV). The first zinc ion (gray circle) is held by a CCCH motif and the second zinc ion is held by a CSCH motif. Green, Loop1 and Loop2. Bottom: estimated amino acid sequence conservation of Loop1 and Loop2 (residues 123–140) is shown. Asterisks indicate the residues S124, N138, and T139 that we selected for mutagenesis.
- (D) Top: schematic of construct to enable Dox-inducible expression of the mutant UPF1^{S124A/N138A/T139A}. This construct was used to generate the clonal myoblast cell line MB135-Tet-UPF1^{S124A/N138A/T139A}. Bottom: immunoblot for total and transgenic UPF1 protein from MB135-Tet-UPF1^{WT} and MB135-Tet-UPF1^{S124A/N138A/T139A} cells 12 hr following transgene induction with Dox is shown. H3, loading control histone H3.
- (E) Schematic of co-immunoprecipitation (coIP) experiments with cell lysates from MB135-Tet-UPF1^{WT} or MB135-Tet-UPF1^{S124A/N138A/T139A} cells. Induced or uninduced cells were treated with MG132 for 6 hr to inhibit the proteasome. IP eluates from each pull-down were then probed with antibodies against UPF1 and MYOD. Ub, ubiquitin.
- (F) Immunoblots of input and IP eluates from (E). Left: input total lysates were probed for UPF1, MYOD, and Ubiquitin. Right: from top to bottom, IP eluates from the anti-UPF1, anti-MYOD, and anti-Ubiquitin pull-downs were probed for UPF1 and MYOD.
- (G) As in (E), but induced cells were treated or not treated with MG132 for 6 hr to inhibit the proteasome. IP eluates from the anti-MYOD pull-down were probed with antibodies against UPF1 and Ubiquitin.
- (H) Immunoblots of input and IP eluates from (G). Left: input total lysates were probed for UPF1, MYOD, and Ubiquitin. Right: IP eluates from the anti-MYOD pull-down were probed for UPF1, MYOD, and Ubiquitin. Bar plots, quantification of UPF1 (top) or MYOD-Ub (bottom) in coIP with MYOD relative to the level of MYOD IP.

See also Figure S3.

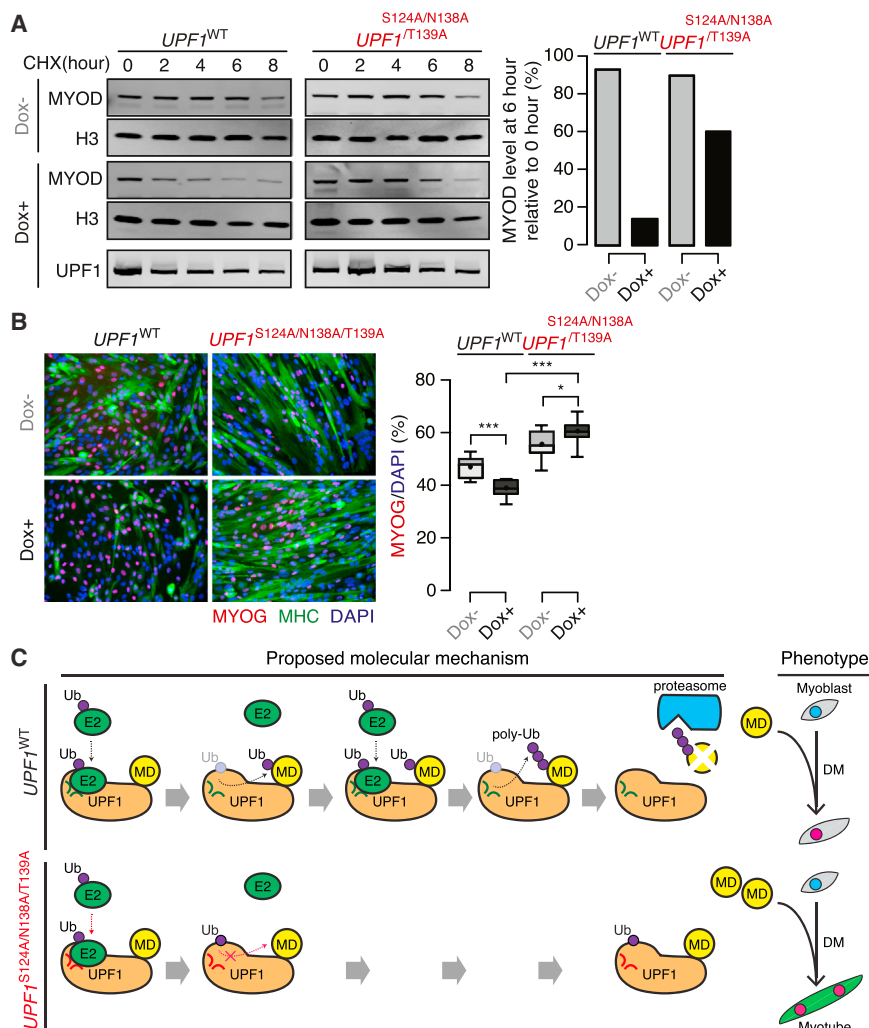


Figure 7. UPF1 RING Domain Mutations Stabilize MYOD Protein and Promote Myogenesis

(A) Immunoblot for MYOD protein, measured throughout a time course following cycloheximide (CHX, 100 μ g/mL) treatment to inhibit translation. Identical numbers of induced or uninduced MB135-Tet-UPF1^{WT} or MB135-Tet-UPF1^{S124A/N138A/T139A} cells were used. H3, loading control histone H3. H3 has a long half-life (Toyama et al., 2013). Lower blot: levels of induced UPF1^{WT} and UPF1^{S124A/N138A/T139A} proteins are shown.

(B) Immunofluorescence labeling of induced or uninduced MB135-Tet-UPF1^{WT} or MB135-Tet-UPF1^{S124A/N138A/T139A} cells with antibodies against MYOG (red) and MHC (green) at day 2. Boxplot, percentage of MYOG⁺ nuclei measured over ten fields; whiskers, maximum and minimum over the fields. *p < 0.05, **p < 0.01, ***p < 0.001.

(C) Schematic of proposed interactions between UPF1 and MYOD (MD) during myogenesis. The E3 ligase activity of UPF1's RING domain promotes proteasome-mediated degradation of MYOD protein in myoblasts. Mutating the E2-E3 binding pocket of UPF1 stabilizes MYOD protein, which in turn promotes myogenesis. Green versus red loops within UPF1 indicate the wild-type versus mutated E2-E3 binding pockets. Black versus red dotted arrows indicate proposed RING domain activities for wild-type versus mutated UPF1, including recruiting an E2 conjugase and transferring ubiquitin (Ub) for the wild-type protein. DM, differentiation media. See also Figure S4.

seem to be involved in degrading peptide products encoded by NMD substrates (Verma et al., 2013). However, deletion of Upf1 or the E3 ligase Ubr1 stabilized

that are subjected to proteolytic decay, as well as to test the hypothesis that UPF1's E3 activity governs this process.

UPF1's mechanistic role in both RNA and protein decay supports the conjecture that activation of translation-dependent mRNA quality control frequently results in peptide as well as mRNA degradation (Brandman and Hegde, 2016). Such direct connections between mRNA and protein quality control have been clearly elucidated for the ribosome quality control complex (RQC). The RQC is a ribosome-associated quality control mechanism that degrades nascent peptides encoded by mRNAs lacking termination codons or containing rare codons, stem loops, or other barriers to efficient translation (Brandman et al., 2012). These difficult-to-translate mRNA templates can induce ribosome stalling (Shao et al., 2013). The RQC may then recognize this stalled ribosome (Becker et al., 2011), split it into its constituent subunits (Shoemaker et al., 2010), expose the mRNA for endonucleolytic cleavage and/or exosome-mediated decay (Doma and Parker, 2006; van Hoof et al., 2002), and catalyze ubiquitination and degradation of the nascent peptide via the RING E3 ligase Listerin (Bengtson and Joazeiro, 2010). The canonical RQC components, including the E3 ligase Listerin, do not

NMD substrate-encoded peptides in yeast, suggesting that Upf1 and/or Ubr1's E3 ligase activities contribute to the degradation of these aberrant peptides (Verma et al., 2013). It remains to be determined whether UPF1 and/or UBR1 promote degradation of NMD substrate-encoded peptides in human cells.

MYOD is probably not the only normally occurring protein that is targeted for regulated degradation in a UPF1-dependent manner. Just as UPF1 plays basal cytoprotective as well as regulatory roles in mRNA degradation, so may UPF1's E3 activity result in the degradation of abnormal peptides encoded by NMD substrates as well as normally occurring, well-formed proteins. Determining which specific features of MYOD mRNA and/or protein result in UPF1-dependent MYOD proteolysis may aid in the identification of other normally occurring proteins whose turnover is regulated by UPF1.

Finally, our results suggest that disease-associated perturbations of UPF1 may dysregulate protein quality control in addition to RNA surveillance. Impaired UPF1 function and/or NMD has been identified in genetic diseases, cancer, and viral infection. For example, the disease gene *DUX4*, which causes facio-scapulohumeral muscular dystrophy, triggers UPF1 proteolysis

(Feng et al., 2015); *UPF1* is commonly subject to somatic mutations in pancreatic adenocarcinoma (Liu et al., 2014) and inflammatory myofibroblastic tumors (Lu et al., 2016); and the hepatitis C virus core protein interacts with a component of the exon-junction complex and disrupts NMD (Ramage et al., 2015). In each case, perturbations in *UPF1* or associated NMD factors may inhibit normal protein decay as well as RNA decay, potentially implicating impaired protein quality control in these diseases.

STAR★METHODS

Detailed methods are provided in the online version of this paper and include the following:

- KEY RESOURCES TABLE
- CONTACT FOR REAGENT AND RESOURCE SHARING
- EXPERIMENTAL MODEL AND SUBJECT DETAILS
 - Cell lines
 - Primary myoblast culture
 - Microbe strains
- METHOD DETAILS
 - siRNA transfection
 - Immunofluorescence microscopy
 - RNA and protein extraction
 - Western blotting
 - Real-time qPCR
 - Lentivirus construction and production
 - Transgenic *UPF1* cell line generation
 - RNA-seq library preparation
 - RNA-seq read mapping
 - Gene expression measurement and Gene Ontology enrichment analysis
 - *UPF1* RING domain conservation estimate
 - Actinomycin D chase, MG132 treatment and CHX chase experiments
 - CDC34-HA expression plasmid construction, mammalian cell transfection and co-immunoprecipitation experiments
 - shRNA expressing lentivirus production
 - *UPF1*, MYOD, and ubiquitin co-immunoprecipitation experiments
- QUANTIFICATION AND STATISTICAL ANALYSIS
- DATA AND SOFTWARE AVAILABILITY
 - Experimental data and plasmids
 - Accession codes

SUPPLEMENTAL INFORMATION

Supplemental Information includes four figures and one table and can be found with this article online at <http://dx.doi.org/10.1016/j.molcel.2017.05.034>.

AUTHOR CONTRIBUTIONS

Q.F., S.J., and R.K.B. designed the experiments. Q.F. performed the experiments and created the figures. Q.F., S.J., and R.K.B. analyzed the data. Q.F. and R.K.B. wrote the paper.

ACKNOWLEDGMENTS

We thank Sergey Ovchinnikov for help with interpreting the *UPF1* domain structure, Melissa Conerly for advice with MYOD antibodies, and Stephen Tapscott and Laurie Snider for project feedback and a gift of primary myoblasts. This research was supported by the Ellison Medical Foundation AG-NS-1030-13 (R.K.B.), NIH/NINDS P01 NS069539 (R.K.B.), and the FSH Society FSHS-22014-01 (S.J.).

Received: November 17, 2016

Revised: May 5, 2017

Accepted: May 26, 2017

Published: June 29, 2017

REFERENCES

- Balistreri, G., Horvath, P., Schweingruber, C., Zünd, D., McInerney, G., Merits, A., Mühlemann, O., Azzalin, C., and Helenius, A. (2014). The host nonsense-mediated mRNA decay pathway restricts Mammalian RNA virus replication. *Cell Host Microbe* 16, 403–411.
- Barberan-Soler, S., Lambert, N.J., and Zahler, A.M. (2009). Global analysis of alternative splicing uncovers developmental regulation of nonsense-mediated decay in *C. elegans*. *RNA* 15, 1652–1660.
- Becker, T., Armache, J.-P., Jarasch, A., Anger, A.M., Villa, E., Sieber, H., Motaal, B.A., Mielke, T., Berninghausen, O., and Beckmann, R. (2011). Structure of the no-go mRNA decay complex Dom34-Hbs1 bound to a stalled 80S ribosome. *Nat. Struct. Mol. Biol.* 18, 715–720.
- Bengtson, M.H., and Joazeiro, C.A.P. (2010). Role of a ribosome-associated E3 ubiquitin ligase in protein quality control. *Nature* 467, 470–473.
- Berdsen, C.E., and Wolberger, C. (2014). New insights into ubiquitin E3 ligase mechanism. *Nat. Struct. Mol. Biol.* 21, 301–307.
- Brandman, O., and Hegde, R.S. (2016). Ribosome-associated protein quality control. *Nat. Struct. Mol. Biol.* 23, 7–15.
- Brandman, O., Stewart-Ornstein, J., Wong, D., Larson, A., Williams, C.C., Li, G.-W., Zhou, S., King, D., Shen, P.S., Weibezahn, J., et al. (2012). A ribosome-bound quality control complex triggers degradation of nascent peptides and signals translation stress. *Cell* 151, 1042–1054.
- Brannan, K.W., Jin, W., Huelga, S.C., Banks, C.A.S., Gilmore, J.M., Florens, L., Washburn, M.P., Van Nostrand, E.L., Pratt, G.A., Schwinn, M.K., et al. (2016). SONAR discovers RNA-binding proteins from analysis of large-scale protein-protein interactomes. *Mol. Cell* 64, 282–293.
- Bruno, I.G., Karam, R., Huang, L., Bhardwaj, A., Lou, C.H., Shum, E.Y., Song, H.-W., Corbett, M.A., Gifford, W.D., Gecz, J., et al. (2011). Identification of a microRNA that activates gene expression by repressing nonsense-mediated RNA decay. *Mol. Cell* 42, 500–510.
- Clerici, M., Mourão, A., Gutsche, I., Gehring, N.H., Hentze, M.W., Kulozik, A., Kadlec, J., Sattler, M., and Cusack, S. (2009). Unusual bipartite mode of interaction between the nonsense-mediated decay factors, *UPF1* and *UPF2*. *EMBO J.* 28, 2293–2306.
- Conerly, M.L., Yao, Z., Zhong, J.W., Groudine, M., and Tapscott, S.J. (2016). Distinct activities of Myf5 and MyoD indicate separate roles in skeletal muscle lineage specification and differentiation. *Dev. Cell* 36, 375–385.
- Crooks, G.E., Hon, G., Chandonia, J.-M., and Brenner, S.E. (2004). WebLogo: a sequence logo generator. *Genome Res.* 14, 1188–1190.
- Deshaies, R.J., and Joazeiro, C.A.P. (2009). RING domain E3 ubiquitin ligases. *Annu. Rev. Biochem.* 78, 399–434.
- Doma, M.K., and Parker, R. (2006). Endonucleolytic cleavage of eukaryotic mRNAs with stalls in translation elongation. *Nature* 440, 561–564.
- Feng, Q., Snider, L., Jagannathan, S., Tawil, R., van der Maarel, S.M., Tapscott, S.J., and Bradley, R.K. (2015). A feedback loop between nonsense-mediated decay and the retrogene *DUX4* in facioscapulohumeral muscular dystrophy. *Elife* 4, e04996.

- Flury, V., Restuccia, U., Bachi, A., and Mühlemann, O. (2014). Characterization of phosphorylation- and RNA-dependent UPF1 interactors by quantitative proteomics. *J. Proteome Res.* *13*, 3038–3053.
- Gardner, L.B. (2008). Hypoxic inhibition of nonsense-mediated RNA decay regulates gene expression and the integrated stress response. *Mol. Cell Biol.* *28*, 3729–3741.
- Glögnitzer, J., Akimcheva, S., Srinivasan, A., Kusenda, B., Riehs, N., Stampfl, H., Bautor, J., Dekrout, B., Jonak, C., Jiménez-Gómez, J.M., et al. (2014). Nonsense-mediated mRNA decay modulates immune receptor levels to regulate plant antibacterial defense. *Cell Host Microbe* *16*, 376–390.
- Gong, C., Kim, Y.K., Woeller, C.F., Tang, Y., and Maquat, L.E. (2009). SMD and NMD are competitive pathways that contribute to myogenesis: effects on PAX3 and myogenin mRNAs. *Genes Dev.* *23*, 54–66.
- Hurt, J.A., Robertson, A.D., and Burge, C.B. (2013). Global analyses of UPF1 binding and function reveal expanded scope of nonsense-mediated mRNA decay. *Genome Res.* *23*, 1636–1650.
- Ishibashi, J., Perry, R.L., Asakura, A., and Rudnicki, M.A. (2005). MyoD induces myogenic differentiation through cooperation of its NH₂- and COOH-terminal regions. *J. Cell Biol.* *171*, 471–482.
- Jia, J., Furlan, A., Gonzalez-Hilarion, S., Leroy, C., Gruenert, D.C., Tulasne, D., and Lejeune, F. (2015). Caspases shutdown nonsense-mediated mRNA decay during apoptosis. *Cell Death Differ.* *22*, 1754–1763.
- Kadlec, J., Guilligay, D., Ravelli, R.B., and Cusack, S. (2006). Crystal structure of the UPF2-interacting domain of nonsense-mediated mRNA decay factor UPF1. *RNA* *12*, 1817–1824.
- Karam, R., Lou, C.-H., Kroeger, H., Huang, L., Lin, J.H., and Wilkinson, M.F. (2015). The unfolded protein response is shaped by the NMD pathway. *EMBO Rep.* *16*, 599–609.
- Krom, Y.D., Dumonceaux, J., Mamchaoui, K., den Hamer, B., Mariot, V., Negroni, E., Geng, L.N., Martin, N., Tawil, R., Tapscott, S.J., et al. (2012). Generation of isogenic D4Z4 contracted and noncontracted immortal muscle cell clones from a mosaic patient: a cellular model for FSHD. *Am. J. Pathol.* *181*, 1387–1401.
- Kuroha, K., Tatematsu, T., and Inada, T. (2009). Upf1 stimulates degradation of the product derived from aberrant messenger RNA containing a specific nonsense mutation by the proteasome. *EMBO Rep.* *10*, 1265–1271.
- Kuroha, K., Ando, K., Nakagawa, R., and Inada, T. (2013). The Upf factor complex interacts with aberrant products derived from mRNAs containing a premature termination codon and facilitates their proteasomal degradation. *J. Biol. Chem.* *288*, 28630–28640.
- Langmead, B., Trapnell, C., Pop, M., and Salzberg, S.L. (2009). Ultrafast and memory-efficient alignment of short DNA sequences to the human genome. *Genome Biol.* *10*, R25.
- Lewis, B.P., Green, R.E., and Brenner, S.E. (2003). Evidence for the widespread coupling of alternative splicing and nonsense-mediated mRNA decay in humans. *Proc. Natl. Acad. Sci. USA* *100*, 189–192.
- Li, B., and Dewey, C.N. (2011). RSEM: accurate transcript quantification from RNA-seq data with or without a reference genome. *BMC Bioinformatics* *12*, 323.
- Li, T., Shi, Y., Wang, P., Guachalla, L.M., Sun, B., Joerss, T., Chen, Y.-S., Groth, M., Krueger, A., Platzer, M., et al. (2015). Smg6/Est1 licenses embryonic stem cell differentiation via nonsense-mediated mRNA decay. *EMBO J.* *34*, 1630–1647.
- Liu, C., Karam, R., Zhou, Y., Su, F., Ji, Y., Li, G., Xu, G., Lu, L., Wang, C., Song, M., et al. (2014). The UPF1 RNA surveillance gene is commonly mutated in pancreatic adenocarcinoma. *Nat. Med.* *20*, 596–598.
- Lorick, K.L., Jensen, J.P., Fang, S., Ong, A.M., Hatakeyama, S., and Weissman, A.M. (1999). RING fingers mediate ubiquitin-conjugating enzyme (E2)-dependent ubiquitination. *Proc. Natl. Acad. Sci. USA* *96*, 11364–11369.
- Lou, C.H., Shao, A., Shum, E.Y., Espinoza, J.L., Huang, L., Karam, R., and Wilkinson, M.F. (2014). Posttranscriptional control of the stem cell and neurogenic programs by the nonsense-mediated RNA decay pathway. *Cell Rep.* *6*, 748–764.
- Lu, J., Plank, T.-D., Su, F., Shi, X., Liu, C., Ji, Y., Li, S., Huynh, A., Shi, C., Zhu, B., et al. (2016). The nonsense-mediated RNA decay pathway is disrupted in inflammatory myofibroblastic tumors. *J. Clin. Invest.* *126*, 3058–3062.
- Lydeard, J.R., Schulman, B.A., and Harper, J.W. (2013). Building and remodeling Cullin-RING E3 ubiquitin ligases. *EMBO Rep.* *14*, 1050–1061.
- Lykke-Andersen, S., and Jensen, T.H. (2015). Nonsense-mediated mRNA decay: an intricate machinery that shapes transcriptomes. *Nat. Rev. Mol. Cell Biol.* *16*, 665–677.
- Martin, L., and Gardner, L.B. (2015). Stress-induced inhibition of nonsense-mediated RNA decay regulates intracellular cystine transport and intracellular glutathione through regulation of the cystine/glutamate exchanger SLC7A11. *Oncogene* *34*, 4211–4218.
- McIlwain, D.R., Pan, Q., Reilly, P.T., Elia, A.J., McCracken, S., Wakeham, A.C., Itie-Youten, A., Blencowe, B.J., and Mak, T.W. (2010). Smg1 is required for embryogenesis and regulates diverse genes via alternative splicing coupled to nonsense-mediated mRNA decay. *Proc. Natl. Acad. Sci. USA* *107*, 12186–12191.
- Metzger, M.B., Pruneda, J.N., Klevit, R.E., and Weissman, A.M. (2014). RING-type E3 ligases: master manipulators of E2 ubiquitin-conjugating enzymes and ubiquitination. *Biochim. Biophys. Acta* *1843*, 47–60.
- Popp, M.W.-L., and Maquat, L.E. (2013). Organizing principles of mammalian nonsense-mediated mRNA decay. *Annu. Rev. Genet.* *47*, 139–165.
- Popp, M.W., and Maquat, L.E. (2015). Attenuation of nonsense-mediated mRNA decay facilitates the response to chemotherapeutics. *Nat. Commun.* *6*, 6632.
- Ramage, H.R., Kumar, G.R., Verschueren, E., Johnson, J.R., Von Dollen, J., Johnson, T., Newton, B., Shah, P., Horner, J., Krogan, N.J., and Ott, M. (2015). A combined proteomics/genomics approach links hepatitis C virus infection with nonsense-mediated mRNA decay. *Mol. Cell* *57*, 329–340.
- Remmert, M., Biegert, A., Hauser, A., and Söding, J. (2011). HHblits: lightning-fast iterative protein sequence searching by HMM-HMM alignment. *Nat. Methods* *9*, 173–175.
- Robinson, M.D., and Oshlack, A. (2010). A scaling normalization method for differential expression analysis of RNA-seq data. *Genome Biol.* *11*, R25.
- Shao, S., von der Malsburg, K., and Hegde, R.S. (2013). Listerin-dependent nascent protein ubiquitination relies on ribosome subunit dissociation. *Mol. Cell* *50*, 637–648.
- Shoemaker, C.J., Eyley, D.E., and Green, R. (2010). Dom34:Hbs1 promotes subunit dissociation and peptidyl-tRNA drop-off to initiate no-go decay. *Science* *330*, 369–372.
- Skaar, J.R., Pagan, J.K., and Pagano, M. (2013). Mechanisms and function of substrate recruitment by F-box proteins. *Nat. Rev. Mol. Cell Biol.* *14*, 369–381.
- Snider, L., Geng, L.N., Lemmers, R.J.L.F., Kyba, M., Ware, C.B., Nelson, A.M., Tawil, R., Filippova, G.N., van der Maarel, S.M., Tapscott, S.J., and Miller, D.G. (2010). Facioscapulohumeral dystrophy: incomplete suppression of a retrotransposed gene. *PLoS Genet.* *6*, e1001181.
- Song, A., Wang, Q., Goebel, M.G., and Harrington, M.A. (1998). Phosphorylation of nuclear MyoD is required for its rapid degradation. *Mol. Cell Biol.* *18*, 4994–4999.
- Takahashi, S., Araki, Y., Ohya, Y., Sakuno, T., Hoshino, S., Kontani, K., Nishina, H., and Katada, T. (2008). Upf1 potentially serves as a RING-related E3 ubiquitin ligase via its association with Upf3 in yeast. *RNA* *14*, 1950–1958.
- Tapscott, S.J., Davis, R.L., Thayer, M.J., Cheng, P.F., Weintraub, H., and Lassar, A.B. (1988). MyoD1: a nuclear phosphoprotein requiring a Myc homology region to convert fibroblasts to myoblasts. *Science* *242*, 405–411.
- Thoren, L.A., Nørgaard, G.A., Weischenfeldt, J., Waage, J., Jakobsen, J.S., Damgaard, I., Bergström, F.C., Blom, A.M., Borup, R., Bisgaard, H.C., and Porse, B.T. (2010). UPF2 is a critical regulator of liver development, function and regeneration. *PLoS ONE* *5*, e11650.

Toyama, B.H., Savas, J.N., Park, S.K., Harris, M.S., Ingolia, N.T., Yates, J.R., 3rd, and Hetzer, M.W. (2013). Identification of long-lived proteins reveals exceptional stability of essential cellular structures. *Cell* 154, 971–982.

Trapnell, C., Pachter, L., and Salzberg, S.L. (2009). TopHat: discovering splice junctions with RNA-seq. *Bioinformatics* 25, 1105–1111.

UniProt Consortium (2012). Reorganizing the protein space at the Universal Protein Resource (UniProt). *Nucleic Acids Res.* 40, D71–D75.

van Hoof, A., Frischmeyer, P.A., Dietz, H.C., and Parker, R. (2002). Exosome-mediated recognition and degradation of mRNAs lacking a termination codon. *Science* 295, 2262–2264.

Verma, R., Oania, R.S., Kolawa, N.J., and Deshaies, R.J. (2013). Cdc48/p97 promotes degradation of aberrant nascent polypeptides bound to the ribosome. *Elife* 2, e00308.

Wagenmakers, E.-J., Lodewyckx, T., Kuriyal, H., and Grasman, R. (2010). Bayesian hypothesis testing for psychologists: a tutorial on the Savage-Dickey method. *Cognit. Psychol.* 60, 158–189.

Wang, D., Zavadil, J., Martin, L., Parisi, F., Friedman, E., Levy, D., Harding, H., Ron, D., and Gardner, L.B. (2011). Inhibition of nonsense-mediated RNA decay by the tumor microenvironment promotes tumorigenesis. *Mol. Cell. Biol.* 31, 3670–3680.

Weischenfeldt, J., Damgaard, I., Bryder, D., Theilgaard-Mönch, K., Thoren, L.A., Nielsen, F.C., Jacobsen, S.E.W., Nerlov, C., and Porse, B.T. (2008). NMD is essential for hematopoietic stem and progenitor cells and for eliminating by-products of programmed DNA rearrangements. *Genes Dev.* 22, 1381–1396.

Young, M.D., Wakefield, M.J., Smyth, G.K., and Oshlack, A. (2010). Gene ontology analysis for RNA-seq: accounting for selection bias. *Genome Biol.* 11, R14.

STAR★METHODS

KEY RESOURCES TABLE

REAGENT or RESOURCE	SOURCE	IDENTIFIER
Antibodies		
Anti-BrdU	Invitrogen	33900
Anti-MYOG	Santa Cruz	M225
Anti-MHC	R&D systems	MF20
2 nd anti-rabbit-TRITC	BD PharMingen	Discontinued
2 nd anti-mouse-FITC	BD PharMingen	554001
Anti-UPF1	Abcam	Ab86057; RRID:AB_1925389
Anti- α -tubulin	Sigma	T9026; RRID:AB_477593
Anti-MYOD	Thermo	5.8A, MA5-12902; RRID:AB_10982953
Anti-MYOD	Abcam	Ab126726; RRID:AB_11130410
Anti-FLAG	Thermo	FG4R, MA1-91878
Anti-H3	Abcam	Ab1791; RRID:AB_302613
Anti-HA	Thermo	2-2.2.14, 26183
Anti-Ubiquitin	Boston Biochem	A-104
IRDye 680RD Goat anti-Rabbit IgG (H + L)	LI-COR	P/N 926-68071
IRDye 680RD Donkey anti-Mouse IgG (H + L)	LI-COR	P/N 926-68072
IRDye 800CW Donkey anti-Rabbit IgG (H + L)	LI-COR	P/N 926-32213
IRDye 800CW Donkey anti-Mouse IgG (H + L)	LI-COR	P/N 926-32212
Bacterial and Virus Strains		
NEB 5-alpha Competent <i>E. coli</i> (High Efficiency)	NEB	C2987H
NEB Stable Competent <i>E. coli</i> (High Efficiency)	NEB	C3040H
Chemicals, Peptides, and Recombinant Proteins		
Insulin	Sigma	I9278
Transferrin	Sigma	T3309
rhFGF	Promega	G5071
Dexamethasone	Sigma	D1756
Puromycin dihydrochloride	Sigma	P9620
Doxycycline hyclate	Sigma	D9891
Actinomycin D	Sigma	A4262
Protease Inhibitor Tablets	Fisher Pierce	88666
DSP	Life Technologies	22585
Polybrene	Sigma	TR-1003
MG132	Sigma	C2211
cycloheximide	Sigma	C7698
Critical Commercial Assays		
Lipofectamine RNAiMAX	Life Technologies	13778150
Lipofectamine 3000	Life Technologies	L3000015
SuperScriptIII First-Strand System	Life Technologies	18080-093
Power SYBR Green Master Mix	Life Technologies	4367659
TruSeq RNA Library Preparation Kit	Illumina	RS-122-2001
Agencourt AMPure XP beads	Beckman Coulter	A63881
Anti-FLAG M2 Magnetic Beads	Sigma	M8823

(Continued on next page)

Continued

REAGENT or RESOURCE	SOURCE	IDENTIFIER
Deposited Data		
RNA-seq data	This paper	GEO: GSE87679
Raw images	This paper, Mendeley Data	http://dx.doi.org/doi:10.17632/z3ff59vm4w.1
Experimental Models: Cell Lines		
54-1 human myoblasts	Krom et al., 2012	N/A
MB135 human myoblasts	Snider et al., 2010	N/A
HEK293T	ATCC	CRL-11268
Primary MB135	Dr. Stephen J. Tapscott	N/A
Primary MB2401	Dr. Stephen J. Tapscott	N/A
MB135-Tet-UPF1 ^{WT}	This paper	N/A
MB135-Tet-UPF1 ^{S124A/N138A/T139A}	This paper	N/A
Oligonucleotides		
Primers for qPCR and cloning, see Table S1	This paper	N/A
siUPF1#1: 5'-GCAGCCACAUUGUAAAUC AUU-3'	Dharmacon, ON-TARGETplus siRNA	J-011763-07
siControl #1	Dharmacon, ON-TARGETplus negative control siRNA	D-001810-03
siUPF1#2: 5'-CAACGGACGUGGAAUA CUtt-3'	Ambion, Silencer Select siRNA	S11928
siControl#2	Ambion, Silencer Select negative control siRNA	4390843
Recombinant DNA		
pCW57.1	Addgene	41393
pCW57.1-Tet-UPF1 ^{WT}	This paper, will be available on Addgene	N/A
pCW57.1-Tet-UPF1 ^{S124A/N138A/T139A}	This paper, will be available on Addgene	N/A
pLKO.1-shUPF1	Dr. Omar Abdel-Wahab	TRCN0000022254
pLKO.1-shNonTargetting	Dr. Omar Abdel-Wahab	N/A
pCMV-VSV-G	Addgene	8454
psPAX2	Addgene	12260
Software and Algorithms		
Bowtie v1.0.0	Langmead et al., 2009	https://github.com/BenLangmead/bowtie
RSEM v.1.2.4	Li and Dewey, 2011	http://deweylab.github.io/RSEM/
TopHat v2.0.8b	Trapnell et al., 2009	https://ccb.jhu.edu/software/tophat/index.shtml
HHblits	Remmert et al., 2011	https://toolkit.tuebingen.mpg.de/

CONTACT FOR REAGENT AND RESOURCE SHARING

Further information and requests for reagents and resources may be directed to and will be fulfilled by the Lead Contact, Dr. Robert K. Bradley, at Fred Hutchinson Cancer Research Center (rbradley@fredhutch.org).

EXPERIMENTAL MODEL AND SUBJECT DETAILS

Cell lines

Three cell lines were used in this study: 54-1 (male), MB135 (female), and HEK293T (female, hypotriploid). Human myoblasts (54-1 and MB135 cells; [Krom et al., 2012](#); [Snider et al., 2010](#)) were cultured in high serum growth media for proliferation below 60% confluence, and induced to differentiate in low serum differentiation media when the cells reached 99% confluence. The growth media was F-10 media-based (GIBCO), and contained 20% fetal bovine serum (GIBCO), 1% penicillin/streptomycin (GIBCO), rhFGF (10 ng/mL, Promega), and dexamethasone (1 μ M, Sigma). The differentiation media was also F-10 media-based (GIBCO), and contained

1% horse serum (GIBCO), 1% penicillin/streptomycin (GIBCO), insulin (10 $\mu\text{g}/\text{mL}$, Sigma), and transferrin (10 $\mu\text{g}/\text{mL}$, Sigma). HEK293T cells used for lentivirus production were obtained from ATCC (CRL-11268) and were cultured in DMEM supplemented with 10% fetal bovine serum (GIBCO) and 1% penicillin/streptomycin (GIBCO). Cells were cultured at 37°C and 5% CO₂. For myoblast cells, fresh growth media was switched every other day, and cells were split when they reached 50% confluence at ratios of 1:2 or 1:4. For HEK293T cells, cells were split twice per week at a 1:10 ratio.

Primary myoblast culture

Early passages of primary myoblasts isolated from individuals MB135 (female) and MB2401 (male) were kind gifts obtained from Dr. Laurie Snider and Dr. Stephen J. Tapscott. Primary myoblasts were cultured under the same conditions as the myoblast cell lines described above. Primary myoblasts were fed with fresh growth media every day. These primary cells can only be maintained for 10 passages.

Microbe strains

NEB 5-alpha Competent *E. coli* (High Efficiency) were obtained from NEB (C2987H). Cells were stored at -80°C and grown in LB medium at 37°C. NEB 5-alpha cells were used for cloning expression plasmids. NEB Stable Competent *E. coli* (High Efficiency) were obtained from NEB (C3040H). Cells were stored at -80°C and grown in LB medium at 30°C. NEB Stable cells were used for production of lentivirus constructs.

METHOD DETAILS

siRNA transfection

siUPF1 #1 (Dharmacon, ON-TARGETplus siRNA J-011763-07), siControl #1 (Dharmacon, ON-TARGETplus negative control siRNA D-001810-03), siUPF1 #2 (Ambion, Silencer Select siRNA s11928), and siControl #2 (Ambion, Silencer Select negative control siRNA 4390843) were transfected with Lipofectamine RNAiMAX (Life Technologies). For transfection in a six-well plate format, 10 nM of siRNA and 6 μL of Lipofectamine RNAiMAX was added on top of cells at 60% confluence in each well. The cells would reach 99% confluence in two days and then be ready for differentiation.

Immunofluorescence microscopy

To assay cell cycle exit by BrdU incorporation, cells were incubated with BrdU-containing media (1 mM/mL, Life Technologies) at 37°C for 1 hr, and then fixed with 4% paraformaldehyde (Electron Microscopy Science) at 4°C for 30 min. To permeabilize fixed cells and break open genomic DNA structure, cells were first incubated with 0.5% Triton X-100-containing PBS, and then with 1N HCl, 2N HCl and 0.1M Borate buffer. For labeling myogenic markers, cells were first fixed with 4% paraformaldehyde at room temperature for 10 min, and then permeabilized with 0.5% Triton X-100-containing PBS. To immunolabel BrdU and myogenic markers after the above preparations, cells were blocked with PBS containing 1% BSA, incubated with primary antibodies in blocking buffer, washed with PBS, and then incubated with secondary antibodies. Antibodies used here were anti-BrdU (Invitrogen, 33900), anti-MYOG (Santa Cruz, M225), anti-MHC (R&D systems, MF20), secondary anti-mouse-FITC (BD PharMingen), and secondary anti-rabbit-TRITC (BD PharMingen). Immunofluorescently labeled cells were viewed and imaged with a ZEISS Axiophot fluorescence microscope. Pictures of ≥ 8 random fields were taken and then analyzed and quantified with ImageJ (Fiji).

RNA and protein extraction

For *UPF1* knockdown and overexpression experiments, cells were lysed in TRIzol (Invitrogen) and RNA and protein were extracted in parallel according to the manufacturer's protocol. Extracted RNA was then cleaned up using the QIAGEN RNeasy Mini Kit. Extracted protein pellets were resuspended in SDS-Tris buffer (5% SDS and 0.5M Tris base) and briefly sonicated. For protein collection only, cells were lysed with RIPA buffer (Cell Signaling) supplemented with protease inhibitor tablets (Fisher Scientific), and then briefly sonicated. Soluble protein was then collected and measured by the bicinchoninic acid (BCA) assay (Thermo).

Western blotting

After determining protein concentrations by the BCA assay, 5 or 10 μg of total protein per sample was used for LI-COR system-based western blotting. After transfer, the nitrocellulose membrane was blocked in the Odyssey blocking buffer. Primary and 800CW IRDye-conjugated secondary antibody incubations were also carried out in the Odyssey blocking buffer. Primary antibodies used were anti-UPF1 (Abcam, ab86057), anti- α -tubulin (Sigma, T9026), anti-MYOD (Thermo, 5.8A, MA5-12902, for knockdown or overexpression experiments; Abcam, ab126726, for MB135-Tet-UPF1^{S124A/N138A/T139A} related experiments), anti-Ubiquitin (Boston Biochem, A-104), anti-FLAG (Thermo, FG4R, MA1-91878), anti-H3 (Abcam, ab1791) and anti-HA (Thermo, 2-2.2.14, 26183).

Real-time qPCR

1 μg of purified RNA per sample was converted into cDNA with the SuperScriptIII First-Strand System (Life Technologies). cDNA was diluted at a 1:50 ratio and used as the template for qPCR. In the final reaction, diluted cDNA was mixed with the 2X Power SYBR Green Master Mix (Life Technologies), together with relevant PCR primers. Primer information for qPCR is provided in [Table S1](#).

Lentivirus construction and production

A UPF1 sequence-verified cDNA clone was ordered from Dharmacon (clone ID 5555509). The UPF1 cDNA was then amplified and cloned into the Dox-inducible lentiviral vector pCW57.1 (Addgene #41393) using the Gibson Assembly Cloning Kit (NEB). Due to high GC content within the first 500 bp of UPF1 cDNA, several attempts to introduce an N-terminal FLAG-tag via PCR primer overhangs failed. The FLAG-tag sequence was therefore introduced after the ATG start codon by replacing the first 381 bp of the UPF1 coding sequence with an in-frame, codon-optimized (lower GC content) gBlock DNA fragment containing the FLAG-tag (IDT). This lentiviral pCW57-FLAG-UPF1^{WT} plasmid was later used as a template to introduce the S124A/N138A/T139A mutations with PCR primers containing mismatched nucleotides that altered the original codons to GCT (Alanine). To produce lentivirus, the lentiviral plasmids pCW57-FLAG-UPF1^{WT} or pCW57-FLAG-UPF1^{S124A/N138A/T139A}, together with the pCMV-VSV-G envelope (Addgene #8454) and the psPAX2 packaging (Addgene #12260) plasmids, were co-transfected into HEK293T cells. For each 10 cm plate of cells, 10 μ g lentiviral plasmid, 2 μ g envelope plasmid, and 2 μ g packaging plasmid was used for calcium phosphate-based transfection. 16 hr after transfection, fresh media (DMEM with 10% cosmic calf serum, GIBCO) containing 1 mM sodium butyrate (Sigma) was changed. 24 hr after changing the media, virus-containing media was collected, filtered through 0.45 μ m filters, and concentrated by centrifuging at 5000 rpm at 4°C for 24 hr. The virus pellet was then resuspended in plain RPMI media (GIBCO), aliquoted, and stored at -80°C. Lentiviral particle preparations were titrated by infecting MB135 cells with a serial dilution of virus and selecting with puromycin (2 ng/mL) for 7 days. Primer information for cloning is provided in [Table S1](#).

Transgenic UPF1 cell line generation

MB135-Tet-UPF1^{WT} and MB135-Tet-UPF1^{S124A/N138A/T139A} cells were generated by transducing MB135 myoblasts with the relevant lentivirus at very low MOI. Starting the day after infection, cells were selected with puromycin (2 ng/mL). After single colonies formed on the low MOI-transduced plates, clones were picked, placed into 24-well plates using sterile cloning cylinders (Sigma, C7983), and expanded. All Dox induction was carried out at 1 μ g/mL.

RNA-seq library preparation

4 μ g of total RNA was collected from 54-1 cells transfected with siUPF1 #1 or a non-targeting siControl #1 two days post-differentiation and used to prepare RNA-seq libraries. Paired-end, poly(A)-selected, unstranded libraries were prepared using the Illumina TruSeq protocol with modifications to select for DNA fragments of length 100-400 bp by varying the bead-to-library ratios (Agencourt AMPure XP beads, Beckman Coulter). Size-selected DNA fragments were then amplified by PCR for 15 cycles and separated on a 2% agarose gel. DNA fragments of length 300 bp were cut out and gel purified using the QIAGEN MinElute gel extraction kit. Bar-coded RNA-seq libraries were sequenced on the Illumina HiSeq 2500 machine, resulting in \sim 100 million paired-end 2 \times 49 bp reads per sample.

RNA-seq read mapping

Reads were mapped to the genome as previously described ([Feng et al., 2015](#)). Briefly, the steps involved were: (1) Map reads to the UCSC hg19 (NCBI GRCh37) genome assembly with Bowtie v1.0.0 ([Langmead et al., 2009](#)) and RSEM v.1.2.4 ([Li and Dewey, 2011](#)) with the '--v2' argument. RSEM was called with the arguments '--bowtie-m 100 --bowtie-chunkmbs 500 --calc-ci --output-genome-bam'. (2) Filter out aligned reads with mapq scores of 0 or splice junction overhangs shorter than 6 bp. (3) Align the remaining unaligned reads with TopHat v2.0.8b ([Trapnell et al., 2009](#)) invoked with the arguments '--bowtie1 --read-mismatches 3 --read-edit-dist 2 --no-mixed --no-discordant --min-anchor-length 6 --splice-mismatches 0 --min-intron-length 10 --max-intron-length 1,000,000 --min-isoform-fraction 0.0 --no-novel-juncs --no-novel-indels --raw-juncs'. (4) Filter TopHat alignments as in step 2. (5) Merge aligned reads reported by RSEM and TopHat.

Gene expression measurement and Gene Ontology enrichment analysis

Gene expression was quantified using RSEM as above. Gene expression values were normalized with the TMM method ([Robinson and Oshlack, 2010](#)), with the scaling factor calculated using protein-coding transcripts only. Genes exhibiting \geq 1.5-fold upregulation with a Bayes factors \geq 100 in the UPF1 KD sample compared to the control KD were identified, where Bayes factors were computed using Wagenmaker's framework ([Wagenmakers et al., 2010](#)). Gene Ontology analysis was performed by comparing upregulated genes to all protein-coding genes with the GSeq method ([Young et al., 2010](#)), using the 'Wallenius' approximation to correct for gene length bias. False discovery rates were then corrected using the Benjamini-Hochberg approach.

UPF1 RING domain conservation estimate

HHblits ([Remmert et al., 2011](#)) was used to generate multiple sequence alignments by querying the following fragment of UPF1 against the UniProt database ([UniProt Consortium, 2012](#)): KDLPIHACSYCGIHDPACVVCNTSKKWFVFCNGRNTSGSHIVNHLV RAKCKEVTLHKDGP. The e-value cutoff used was 1E-10 with four iterations. The generated alignment file was then input into WebLogo ([Crooks et al., 2004](#)) to create the plot of sequence conservation.

Actinomycin D chase, MG132 treatment and CHX chase experiments

To measure MYOD mRNA half-life at day 0 (following transfection of 54-1 cells with siControl #1 or siUPF1 #1), actinomycin D (ActD, Sigma, 2.5 μg/mL) was added to cells to inhibit transcription. After 0, 0.5, 1, 2, 4, 8 and 12 hr of ActD treatment, cells were collected with TRIzol (Invitrogen), RNA was extracted, and qPCR was carried out with primers specific to mature MYOD mRNA. To inhibit the 26S proteasome, MG132 (10 μM) was added to MB135-Tet-UPF1^{WT} cells 12 hr post-Dox induction. After 8 hr of MG132 treatment, identical numbers of cells were collected in RIPA buffer (Cell Signaling) supplemented with protease inhibitor tablets (Fisher Scientific), protein was extracted, and immunoblots for MYOD were performed. To measure MYOD protein levels in MB135-Tet-UPF1^{WT} or MB135-Tet-UPF1^{S124A/N138A/T139A} cells that were or were not treated with Dox to induce transgenic UPF1 expression, cycloheximide (CHX, 100 μg/mL) was added to cells 12 hr post-Dox induction to inhibit translation. After 0, 2, 4, 6 and 8 hr of CHX treatment, identical numbers of cells were collected in RIPA buffer (Cell Signaling) supplemented with protease inhibitor tablets (Fisher Scientific), protein was extracted, and immunoblots for MYOD were performed.

CDC34-HA expression plasmid construction, mammalian cell transfection and co-immunoprecipitation experiments

A CDC34 sequence-verified cDNA clone was ordered from Dharmacon (clone ID 4103120). The CDC34 cDNA was cut out with restriction enzymes EcoRI/XhoI (NEB) and cloned into the mammalian expression vector pUB6/V5-His A (Thermo Fisher Scientific) via ligation. A C-terminal HA-tag was introduced via PCR primer overhangs to generate the pUB6-CDC34-HA construct for transfection. Primer information for cloning is provided in [Table S1](#). To assay UPF1 interaction with CDC34, MB135-Tet-UPF1^{WT} and MB135-Tet-UPF1^{S124A/N138A/T139A} cells were transfected with the pUB6-CDC34-HA construct 48 hr prior to induction of transgenic UPF1 expression by adding or not adding Dox for 12 hr. Two 15 cm plates of cells at ~60% confluence were used per condition. Each 15 cm plate was transfected with 45 μg of DNA using the Lipofectamine 3000 Reagent (Thermo Fisher Scientific). To collect cell lysates for FLAG immunoprecipitation, cells were trypsinized, washed twice with PBS, and cross-linked with DSP (Thermo Fisher Scientific). Cross-linking was terminated by quenching with 20 mM Tris-Cl pH 7.4 in PBS. After one more PBS wash, cells were lysed in 1 mL pre-chilled NET-2 lysis buffer (50 mM Tris-Cl pH 7.4, 150 mM NaCl and 0.05% NP-40) supplemented with phosphatase and protease inhibitor tablets (Fisher Scientific), followed by brief sonication (3 × 10 s) and incubation on ice (15 min). Cell lysates were collected after removing cell debris by centrifugation (10,000 g at 4°C for 15 min) and protein concentrations were determined with the Qubit Protein Assay Kit (Fisher Scientific). 50 μL of lysates per sample were saved as inputs. To pull-down the transgenic FLAG-tagged UPF1, 40 μL of anti-FLAG M2 Magnetic Beads (Sigma) was combined with 1.2 mg of lysates and incubated overnight with rotation at 4°C. To collect IP eluates, the protein-antibody-beads complexes were washed three times with pre-chilled NET-2 buffer, and then directly eluted by suspending beads in 2X SDS sample buffer. 20 μg of inputs and half of IP eluates per sample were used for the downstream immunoblotting experiments.

shRNA expressing lentivirus production

Lentiviral plasmids expressing either a non-targeting control shRNA (GCGCGATAGCGCTAATAATTT, Sigma-Aldrich) or a UPF1 3'UTR-targeting shRNA (GCATCTTATTCTGGGTAATAA, TRCN0000022254) were obtained as kind gifts from Dr. Omar Abdel-Wahab. Similar to concentrated lentivirus production above, to produce fresh lentivirus for efficient shRNA delivery and endogenous UPF1 knock-down, HEK293T cells on each 10 cm plates, were co-transfected with 10 μg lentiviral plasmid, 2 μg envelope plasmid, and 2 μg packaging plasmid. 16 hr after transfection, fresh myoblast growth media (F-10 (GIBCO) with 20% fetal bovine serum (GIBCO), 1% penicillin/streptomycin (GIBCO), rhFGF(10 ng/mL, Promega), and dexamethasone (1 μM, Sigma)) was changed onto HEK293T cells. 24 hr later, virus-containing myoblast growth media was collected, filtered through 0.45 μm filters, mixed with Polybrene (8 μg/mL, Sigma), and added onto myoblasts ready for shRNA experiments.

UPF1, MYOD, and ubiquitin co-immunoprecipitation experiments

Interactions between UPF1 and MYOD and MYOD ubiquitination were assayed as follows. 24 hr before collection, MB135-Tet-UPF1^{WT} and MB135-Tet-UPF1^{S124A/N138A/T139A} cells were or were not treated with Dox to induce transgenic UPF1; 6 hr before collection, cells were or were not treated with MG132 (Sigma, 10 μM) to inhibit the proteasome. Two 15 cm plates of cells at ~60% confluence were used per condition. To collect cell lysates for co-immunoprecipitation, cells were first trypsinized and washed three times with PBS, and then lysed in 1 mL pre-chilled NP40 cell lysis buffer (Fisher Scientific) supplemented with phosphatase and protease inhibitor tablets (Fisher Scientific), followed by brief sonication (3 × 10 s) and incubation on ice (15 min). Cell lysates were collected after removing cell debris by centrifugation (10,000 g at 4°C for 15 min), and protein concentrations were determined with the Qubit Protein Assay Kit (Fisher Scientific). To prepare antibody-coupled magnetic beads, the following antibodies were used: anti-UPF1 (Abcam, ab86057), anti-MYOD (Abcam, ab126726), and anti-Ubiquitin (BostonBiochem, A-104). 1.5 μg of antibody was incubated with 50 μL protein G-coupled Dynabeads (Fisher Scientific) for each IP. For each IP, 0.2 mg of lysates from each condition were added to the 1.5 μg antibody-coupled 50 μL beads and incubated overnight with rotation at 4°C. To collect IP eluates, the protein-antibody-beads complexes were washed three times, transferred to new tubes to avoid elution of unspecific proteins bound to the tube wall, and then eluted in 20 μL of elution buffer by incubating with rotation for 2 min at room temperature. One third of IP eluates per sample were used for the downstream immunoblotting experiments.

QUANTIFICATION AND STATISTICAL ANALYSIS

As described above, differentially expressed genes were identified from the RNA-seq using a Bayesian statistical framework. Bayes factors were computed using Wagenmaker's framework (Wagenmakers et al., 2010). Gene Ontology (GO) enrichment analyses for differentially expressed genes were performed using the GSeq method to correct for biases introduced by transcript length and expression (Young et al., 2010). False discovery rates for GO enrichment analyses were corrected using the Benjamini-Hochberg approach.

Statistical analyses for experimental data, including qPCR data (three replicates performed per experiment) and immunofluorescence microscopy data (eight to ten fields analyzed per experiment), were performed as follows. We computed p -values for a difference in distribution between two samples (e.g., control versus *UPF1* KD) with a two-tailed t -test. The resulting p -values were graphically illustrated in figures with asterisks as described in figure legends.

Error bars in bar plots illustrating qPCR results represent the estimated mean \pm standard deviation. Boxplots illustrating immunofluorescence microscopy analyses represent the second and the third quartiles with two different shaded boxes, wherein the black dot indicates the mean and the error bars indicate the maximum and minimum over the measured data.

DATA AND SOFTWARE AVAILABILITY

Experimental data and plasmids

Raw experimental data from this study have been deposited to Mendeley Data and are available at <http://dx.doi.org/doi:10.17632/z3ff59vm4w.1>. Relevant plasmids are available through Addgene (https://www.addgene.org/Robert_Bradley/).

Accession codes

The accession number for the FASTQ files from the RNA-seq experiments reported in this paper is GEO: GSE87679.